JACS
JOURNAL OF THE AMERICAN CHEMICAL SOCIETY

ARTICLE

pubs.acs.org/JACS

Multifunctional Compact Zwitterionic Ligands for Preparing Robust Biocompatible Semiconductor Quantum Dots and Gold Nanoparticles

Kimihiro Susumu,*[,†] Eunkeu Oh,[†] James B. Delehanty,[‡] Juan B. Blanco-Canosa,[§] Brandy J. Johnson,[‡] Vaibhav Jain,[†] William Judson Hervey, IV,[‡] W. Russ Algar,[‡,∥] Kelly Boeneman,[‡] Philip E. Dawson,[§] and Igor L. Medintz*[,‡]

[†]Optical Sciences Division, Code 5611, [‡]Center for Bio/Molecular Science and Engineering, Code 6900, U.S. Naval Research Laboratory, Washington, D.C. 20375, United States

[§]Departments of Cell Biology and Chemistry, The Scripps Research Institute, La Jolla, California 92037, United States

[∥]College of Science, George Mason University, Fairfax, Virginia 22030, United States

Supporting Information

ABSTRACT: We describe the synthesis of a series of four different ligands which are used to prepare hydrophilic, biocompatible luminescent quantum dots (QDs) and gold nanoparticles (AuNPs). Overall, the ligands are designed to be compact while still imparting a zwitterionic character to the NPs. Ligands are synthesized appended to a bidentate dihydrolipoic acid- (DHLA) anchor group, allowing for high-affinity NP attachment, and simultaneously incorporate tertiary amines along with carboxyl and/or hydroxyl groups. These are placed in close proximity within the ligand structure and their capacity for joint ionization imparts the requisite zwitterionic nature to the nanocrystal. QDs functionalized with the four different compact ligands were subjected to extensive physical characterization including surface charge, wettability, hydrodynamic size, and tolerance to a wide pH range or high salt concentration over time. The utility of the compact ligand coated QDs was further examined by testing of direct conjugation to polyhistidine-appended protein and peptides, aqueous covalent-coupling chemistry, and the ability to engage in Förster resonance energy transfer (FRET). Conjugating cell penetrating peptides to the compact ligand coated QD series facilitated their rapid and efficient cellular uptake, while subsequent cytotoxicity tests showed no apparent decreases in cell viability. *In vivo* biocompatibility was also demonstrated by microinjecting the compact ligand coated QDs into cells and monitoring their stability over time. Inherent benefits of the ligand design could be extended beyond QDs as AuNPs functionalized with the same compact ligand series showed similar colloidal properties. The strong potential of these ligands to expand NP capabilities in many biological applications is highlighted.

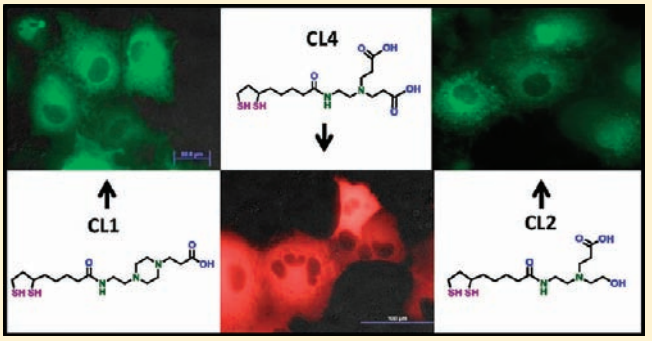

INTRODUCTION

Development of biocompatible nanoparticles (NPs) that exploit the unique size-dependent properties of their constituent materials in a biological context continues to be a major priority in bionanotechnology.[1−8] This goal, in turn, is almost completely dependent upon the properties of the surface 'ligands' utilized to provide aqueous stability to the NPs and facilitate their integration within biological systems. Many different families of ligand molecules are currently being utilized for these purposes with each usually providing its own set of functional benefits and liabilities.[9,10] Besides providing long-term colloidal stability across a wide pH and buffer range to myriad types of monodispersed NPs, the ligands should also have the following features: (i) easily synthesized in bulk quantities; (ii) have a small size that minimizes the hydrodynamic radius of the subsequently functionalized NP; (iii) have high-affinity attachment to the NP while still allowing other molecules access to the NP surface; (iv) provide an available 'handle' for further chemical modification in a relatively simple manner; (v) have minimal undesired interactions with other molecules native to biological environments, that is, opsonization; (vi) have minimal to no toxicity after *in vivo* administration; and finally, (vii) minimally perturb inherent NP properties or those of an attached biomolecule. Although all are important, it has been extremely challenging to design NP ligands that can provide a majority of these properties, let alone all, in a single molecule. Ligands do vary widely in structure and, beyond being utilized for direct NP synthesis, their interactions with NPs can be loosely grouped into two functional mechanisms. The first is encapsulation with amphiphilic polymeric ligands or similar dendrimeric materials that interact with and overcoat the native surface while simultaneously

Received: March 2, 2011
Published: May 25, 2011

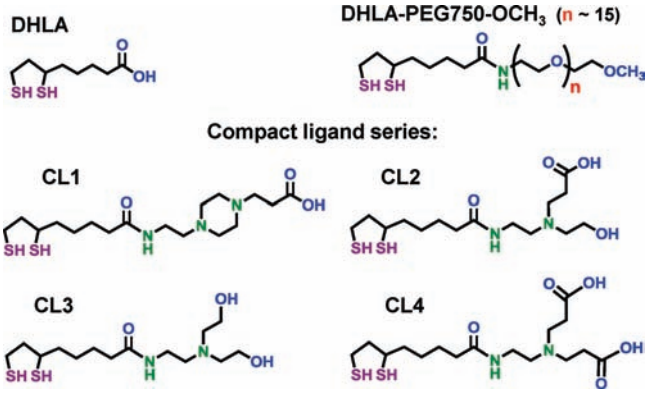

Figure 1. Chemical structures of DHLA and the DHLA-based ligands used in this study. DHLA-PEG750-OCH_3 was synthesized as previously described.[25,26]

mediating colloidal stability. This, however, usually comes at the expense of a much larger hydrodynamic size.[11] In contrast, cap exchange replaces the original hydrophobic surface ligands with bifunctional hydrophilic ligands via mass action to render the NPs water-soluble while keeping relatively small hydrodynamic size.[9−11]

Our research has focused on developing hydrophilic luminescent semiconductor nanocrystals or quantum dots (QDs) for a variety of biological applications including use in cellular delivery, biosensing, functional nanodevices, and as multiplexed probes.[4,9,12−15] This goal has required a parallel focus on developing improved ligands for the QDs. The first generation of ligand utilized dihydrolipoic acid (DHLA), see Figure 1.[16] In comparison to monothiol-ligands which suffer from a high dynamic dissociation rate and thus provide poor long-term colloidal stability to QDs, the bidentate-thiols essentially function as cooperative anchoring groups that strongly coordinate to the nanocrystal surface with the charged carboxyl group at the molecule's other end mediating colloidal stability.[16] This ligand is easily prepared in one step from commercially available thioctic acid (TA) by reduction of the terminal disulfide with sodium borohydride ($NaBH_4$). Importantly, the small, compact size of DHLA ligands also allows direct self-assembly of a variety of oligohistidine-tagged (His-tagged) peptides, proteins, and DNA onto the QD surface.[17−21] However, aqueous solubility of DHLA-coated QDs relies exclusively on deprotonation of the terminal carboxyl groups and their colloidally stable pH window is limited to the basic regime. In contrast, amine-coated QDs are colloidally stable at moderately acidic pH; however, their stability drops when moving from neutral to basic conditions.[22] The second generation of ligand mediated solubility by appending poly(ethylene glycol) (PEG) moieties (molecular weight ranging from 400 up to 1000) to the DHLA anchor group and provided QDs with a much wider range of pH stability.[23] Improvements to this ligand design were more modular in nature and replaced an internal acid-labile ester linkage with an amide bond and provided the option of a wide range of terminal functional groups ranging from biotin to a primary amine, carboxyl, or methoxy, the former of which allows for bioconjugation and covalent modifications.[24−27] Subsequent work demonstrated that the benefits of this PEGylated-ligand design could also be extended to gold nanoparticles (AuNPs).[25,28−30] While the PEG chain extended pH and intracellular stability of the QDs, the long chain length of the PEG unit increased the QD's hydrodynamic size and prohibited conjugation of His-tagged proteins directly onto the QD surface.[18,23,31]

Here, we report the design, synthesis, and functional characterization of a new family of DHLA-based compact ligands which can provide QDs with extended pH and salt stability without increasing their apparent hydrodynamic sizes. In contrast to utilizing a carboxyl or PEG moiety to mediate colloidal stability, this ligand design relies on an inherent zwitterionic nature; chemical structures for the surface compact ligand series (**CL1** ∼ **CL4**) are shown in Figure 1. Characterization of QDs coated with the compact ligands (**CL**-QDs) included examining surface charge, wettability, hydrodynamic volumes, pH and salt stability, testing direct conjugation of His-tagged proteins and peptides, aqueous covalent-coupling chemistry, cellular microinjection and peptide-mediated cellular uptake, cellular imaging, and cytotoxicity. We also demonstrate that the properties of this compact ligand series can be extended to AuNPs in a similar fashion.

MATERIALS AND METHODS

Chemicals. Thioctic acid, 1,1′-carbonyldiimidazole, *N*-(2-aminoethyl)-piperazine, and methyl acrylate were purchased from Acros Organics (Fisher Scientific, Pittsburgh, PA). Lithium hydroxide was purchased from Sigma-Aldrich (St. Louis, MO). Sodium borohydride was purchased from MP Biomedicals (Solon, OH). *N*-(2-Hydroxyethyl)-ethylenediamine and ethylenediamine were purchased from TCI America (Portland, OR). *N*,*N*-Bis(2-hydroxyethyl)ethylenediamine was purchased from Alfa Aesar (Ward Hill, MA). *N*-Ethyl-*N*′-(3-dimethylaminopropyl)-carbodiimide hydrochloride (EDC) and *N*-hydroxysulfosuccinimide (sulfo-NHS) were purchased from Pierce Biotechnology (Rockford, IL). Agarose (low EEO) was purchased from Fisher Scientific. All the other chemicals including solvents were purchased from Sigma Aldrich or Acros Organics and used as received. Phosphate buffered saline (PBS) contains 137 mM NaCl, 10 mM phosphate, and 3 mM KCl (pH 7.4).

Quantum Dots and Gold Nanoparticles. The 550 nm emitting CdSe-ZnS core−shell QDs were synthesized as previously described with some modifications.[32,33] The native surface-coating ligands after the ZnS overcoating step are expected to be a mixture of *n*-hexylphosphonic acid, trioctylphosphine oxide, and trioctylphosphine. The 615 nm emitting CdSe-CdS-CdZnS-ZnS core−multishell QDs were synthesized via modification of published procedures combining successive ion layer adsorption and reaction (SILAR) with thermal cycling techniques.[34−36] The native surface coating ligands of these multishell QDs following the final ZnS overcoating are expected to be a mixture of *n*-dodecylphosphonic acid, diisooctylphosphinic acid, oleic acid, and trioctylphosphine. Custom Qdot 625 nm emitting ITK organic QDs used in the microinjection studies were a gift from Life Technologies (Eugene, OR). Sodium citrate stabilized 5.8 nm diameter gold nanoparticles (AuNPs) were purchased from Ted Pella (Redding, CA).

Ligand Synthesis. *Compounds **1** and **2**.* Thioctic acid (3.00 g, 1.45×10^{-2} mol) and 1,1′-carbonyldiimidazole (CDI) (2.59 g, 1.60×10^{-2} mol) were added to a 100-mL round-bottom flask, and the mixture was purged with N_2. 30 mL of toluene was added to the mixture by syringe, and the reaction mixture stirred at room temperature for 1 h under N_2. The mixture was transferred to an addition funnel and $CHCl_3$ (20 mL) was further mixed in, and then this solution was added dropwise over 30 min to a mixture of *N*-(2-aminoethyl)piperazine (2.10 mL, 1.59×10^{-2} mol) and 30 mL of $CHCl_3$ in a 250-mL two-neck round-bottom flask cooled in an ice-bath under N_2. The reaction mixture was further stirred at room temperature overnight and transferred to a separatory funnel. $CHCl_3$ (∼100 mL) and deionized (DI) water

(Milli-Q 18 MΩ, ∼100 mL) were added to the mixture and the $CHCl_3$ layer was collected. The aqueous layer was further washed with $CHCl_3$ (2 times). The combined organic layers were dried over Na_2SO_4, filtered, and concentrated to ∼20 mL on a rotary evaporator. The crude product solution was purified over silica gel column chromatography with $CHCl_3$/MeOH (5:1) as the eluent. The product fractions were concentrated to ∼10 mL and directly used for the next reaction.

Product solution was dissolved in 80 mL of MeOH and purged with N_2. Methyl acrylate (5.0 mL, 5.6×10^{-2} mol) was added dropwise and the reaction mixture stirred at room temperature overnight under N_2. The solvent and excess methyl acrylate was subsequently evaporated, and the residue was separated by chromatography on silica gel with $CHCl_3$/MeOH (20:1) as the eluent. Yield = 3.448 g (59% in two steps based on 3.00 g of thioctic acid). *N*-[2-(1-Piperazinyl)ethyl]-5-(1,2-dithiolan-3-yl)pentanamide (**1**): ^{1}H NMR (400 MHz, $CDCl_3$): δ 6.05 (br s, 1H, NH), 3.52−3.63 (m, 1H), 3.35 (q, 2H, J = 7.6 Hz, $-CH_2-$), 3.07−3.23 (m, 2H), 2.89 (t, 4H, J = 6.4 Hz, $-CH_2-$), 2.37−2.53 (m, 7H), 2.20 (t, 2H, J = 10.0 Hz, $-CH_2-CO-$), 1.86−1.97 (m, 1H), 1.55−1.8 (m, 4H), 1.4−1.55 (m, 2H). Product was confirmed by electrospray ionization mass spectrometry (ESI MS) with a mass-to-charge ratio (m/z) of 318.1743 $(M + H)^+$/theoretical protonated monoisotopic mass $(M + H)^+$ was 318.167. *N*-{2-[4-(methoxycarbonylethyl) piperazin-1-yl]ethyl}-5-(1,2-dithiolan-3-yl)pentanamide (**2**): ^{1}H NMR (400 MHz, $CDCl_3$): δ 6.08 (br s, 1H, NH), 3.69 (s, 3H, $-OCH_3$), 3.52−3.63 (m, 1H), 3.34 (q, 2H, J = 7.6 Hz, $-CH_2-$), 3.07−3.23 (m, 2H), 2.71 (t, 2H, J = 9.6 Hz, $-CH_2-$), 2.40−2.58 (m, 13H, $-CH_2-$), 2.20 (t, 2H, J = 9.8 Hz, $-CH_2-CO-$), 1.86−1.97 (m, 1H), 1.6−1.8 (m, 4H), 1.4−1.55 (m, 2H). ESI MS m/z: 404.2018 $(M + H)^+$/ theoretical protonated monoisotopic mass 404.204.

*Compounds **4** and **5***. Thioctic acid (4.00 g, 1.94×10^{-2} mol) and CDI (3.46 g, 2.13×10^{-2} mol) were added to a 100-mL round-bottom flask, and the mixture was purged with N_2. 50 mL of $CHCl_3$ was added to the mixture by syringe and the reaction mixture stirred at room temperature for 1 h under N_2. The mixture was then transferred to an addition funnel where 20 mL of $CHCl_3$ was further mixed in, and the resulting solution was added dropwise over 30 min to a mixture of *N*-(2-hydroxyethyl)ethylenediamine (2.20 mL, 2.18×10^{-2} mol) and 40 mL of $CHCl_3$ in a 250-mL two-neck round-bottom flask cooled in an ice-bath under N_2. The reaction mixture was further stirred at room temperature for 5 h and transferred to a separatory funnel. Saturated sodium bicarbonate solution (∼100 mL) was added to the mixture and the $CHCl_3$ layer was collected. The aqueous layer was further washed with $CHCl_3$ (4 times). The combined organic layers were dried over Na_2SO_4, filtered, and concentrated to ∼20 mL by rotary evaporator. The crude product solution was purified by chromatography on silica gel with $CHCl_3$/MeOH (5:1) as the eluent. The product fractions were concentrated to ∼10 mL and used for the next reaction.

Product solution was dissolved in 80 mL of MeOH and purged with N_2. Methyl acrylate (9.0 mL, 0.10 mol) was added dropwise and the reaction mixture was stirred at room temperature overnight under N_2. The solvent and excess methyl acrylate were evaporated. The residue was again purified by chromatography on silica gel with $CHCl_3$/MeOH (10:1) as the eluent. Yield = 3.584 g (49% in two steps based on 4.00 g of thioctic acid). *N*-{2-[(2-Hydroxyethyl)amino]ethyl}-5-(1,2-dithiolan-3-yl)pentanamide (**4**): ^{1}H NMR (400 MHz, $CDCl_3$): δ 5.97 (br s, 1H, NH), 3.68 (t, 2H, J = 6.8 Hz, $-CH_2-$), 3.53−3.62 (m, 1H), 3.37 (q, 2H, J = 7.6 Hz, $-CH_2-$), 3.07−3.23 (m, 2H), 2.79 (t, 2H, J = 6.8 Hz, $-CH_2-$), 2.78 (t, 2H, J = 7.8 Hz, $-CH_2-$), 2.41−2.52 (m, 1H), 2.20 (t, 2H, J = 9.8 Hz, $-CH_2-CO-$), 1.86−1.97 (m, 1H), 1.55−1.8 (m, 4H), 1.4−1.55 (m, 2H). ESI MS m/z: 293.1206 $(M + H)^+$/theoretical protonated monoisotopic mass 293.136. *N*-{2-[*N*′-(2-Hydroxyethyl)-*N*′-(methoxycarbonylethyl)amino]ethyl}-5-(1,2-dithiolan-3-yl)pentanamide (**5**): ^{1}H NMR (400 MHz, $CDCl_3$): δ 6.39 (br s, 1H, NH), 3.72 (s, 3H, $-OCH_3$), 3.52−3.63 (m, 3H), 3.33 (q, 2H, J = 7.6 Hz, $-CH_2-$), 3.07−3.23 (m, 2H), 2.80 (q, 2H, J = 8.2 Hz, $-CH_2-$), 2.60 (q, 4H, J = 6.8 Hz, $-CH_2-$), 2.49 (t, 2H, J = 8.0 Hz, $-CH_2-$), 2.41−2.53 (m, 1H), 2.21 (t, 2H, J = 10.0 Hz, $-CH_2-CO-$), 1.86−1.97 (m, 1H), 1.6−1.8 (m, 4H), 1.4−1.55 (m, 2H). ESI MS m/z: 379.1720 $(M + H)^+$/theoretical protonated monoisotopic mass 379.173.

*Compound **7***. Thioctic acid (2.00 g, 9.69×10^{-3} mol) and CDI (1.73 g, 1.07×10^{-2} mol) were added to a 100-mL round-bottom flask, and the mixture was purged with N_2. 20 mL of $CHCl_3$ was added to the mixture by syringe and the reaction mixture stirred at room temperature for 1 h under N_2. The mixture above was transferred to an addition funnel and 5.0 mL of $CHCl_3$ was further mixed in, and the resulting solution added dropwise over 30 min to a mixture of *N*,*N*-bis(2-hydroxyethyl)ethylenediamine (1.60 g, 1.08×10^{-2} mol) and 20 mL of $CHCl_3$ in a 250-mL two-neck round-bottom flask under N_2. The reaction mixture was further stirred at room temperature overnight and poured into DI water (∼100 mL). The $CHCl_3$ layer was collected and the product was further extracted with $CHCl_3$ (2 times). The combined organic layers were dried over Na_2SO_4 and filtered. The solvent was evaporated and the crude product was purified by chromatography on silica gel with $CHCl_3$/MeOH (20:1) as the eluent. Yield = 2.614 g (80% based on 2.00 g of thioctic acid). *N*-{2-[*N*′,*N*′-Bis(2-hydroxyethyl)amino]ethyl}-5-(1,2-dithiolan-3-yl)pentanamide (**7**): ^{1}H NMR (400 MHz, $CDCl_3$): δ 6.36 (br s, 1H, NH), 3.63 (t, 4H, J = 6.8 Hz, $-CH_2-$), 3.53−3.62 (m, 1H), 3.36 (q, 2H, J = 7.6 Hz, $-CH_2-$), 3.07−3.23 (m, 2H), 2.63−2.73 (m, 6H, $-CH_2-$), 2.41−2.52 (m, 1H), 2.21 (t, 2H, J = 10.0 Hz, $-CH_2-CO-$), 1.86−1.97 (m, 1H), 1.55−1.8 (m, 4H), 1.4−1.55 (m, 2H). ESI MS m/z: 337.1788 $(M + H)^+$/theoretical protonated monoisotopic mass 337.162.

*Compounds **8** and **9***. Thioctic acid (3.00 g, 1.45×10^{-2} mol) and CDI (2.59 g, 1.60×10^{-2} mol) were added to a 100-mL round-bottom flask and the mixture purged with N_2. 30 mL of $CHCl_3$ was added to the mixture by syringe and the reaction mixture stirred at room temperature for 1 h under N_2. The reaction solution was then transferred to an addition funnel and added dropwise over 1 h to a mixture of ethylenediamine (8.0 mL, 0.12 mol) and 30 mL of $CHCl_3$ in a 250-mL two-neck round-bottom flask at room temperature under N_2. The reaction mixture was further stirred at room temperature overnight and transferred to a separatory funnel. DI water (∼100 mL) was added to the mixture and the $CHCl_3$ layer was collected. The aqueous layer was further washed with $CHCl_3$ (3 times). The combined organic layers were concentrated to ∼20 mL and the crude product solution was purified by chromatography on silica gel with $CHCl_3$/MeOH (5:1) as the eluent. The product fractions were concentrated to ∼15 mL and used for the next reaction step.

Product solution was dissolved in 70 mL of MeOH and purged with N_2. Methyl acrylate (10.0 mL, 0.11 mol) was added dropwise and the reaction mixture was stirred at room temperature for 2 days under N_2. The solvent and excess methyl acrylate was evaporated. The residue was separated by chromatography on silica gel with $CHCl_3$/MeOH (20:1) as the eluent. Yield = 3.919 g (64% in 2 steps based on 3.00 g of thioctic acid). *N*-(2-Aminoethyl)-5-(1,2-dithiolan-3-yl)pentanamide (**8**): ^{1}H NMR (400 MHz, $CDCl_3$): δ 6.06 (br s, 1H, NH), 3.53−3.62 (m, 1H), 3.31 (q, 2H, J = 7.7 Hz, $-CH_2-$), 3.07−3.26 (m, 2H), 2.84 (t, 2H, J = 7.8 Hz, $-CH_2-$), 2.41−2.52 (m, 1H), 2.21 (t, 2H, J = 10.0 Hz, $-CH_2-CO-$), 1.86−1.97 (m, 1H), 1.6−1.8 (m, 4H), 1.4−1.6 (m, 2H). ESI MS m/z: 249.0941 $(M + H)^+$/theoretical protonated monoisotopic mass 249.110. *N*-{2-[*N*′,*N*′-Bis(methoxycarbonylethyl)-amino]ethyl}-5-(1,2-dithiolan-3-yl)pentanamide (**9**): ^{1}H NMR (400 MHz, $CDCl_3$): δ 6.52 (br s, 1H, NH), 3.69 (s, 6H, -OCH_3), 3.53−3.63 (m, 1H), 3.33 (q, 2H, J = 7.2 Hz, $-CH_2-$), 3.07−3.22 (m, 2H), 2.74 (t, 4H, J = 8.6 Hz, $-CH_2-$), 2.53 (t, 2H, J = 7.2 Hz, $-CH_2-$), 2.47 (m, 1H), 2.43 (t, 4H, J = 8.6 Hz, $-CH_2-$), 2.22 (t, 2H, J = 9.8 Hz, $-CH_2-CO-$), 1.85−1.97 (m, 1H), 1.6−1.8 (m, 4H), 1.4−1.6 (m, 2H). ESI MS m/z: 421.1647 $(M + H)^+$/theoretical protonated monoisotopic mass 421.183.

Ester Hydrolysis, Ring-Opening, and Cap Exchange of Compact Ligands onto Quantum Dots. Typical procedures for preparing a ligand for cap exchange and the subsequent cap exchange reaction are as follows: LiOH (20.9 mg, 8.71×10^{-4} mol) was added to a mixture of **2** (0.307 g, 7.61×10^{-4} mol), EtOH (2.0 mL), and DI H_2O (1.0 mL). The reaction mixture was stirred at room temperature for 2 h. Completion of ester hydrolysis was checked by TLC (thin layer chromatography) with $CHCl_3$/MeOH (5:1) as the eluent. For reducing the dithiolane group, 4 M HCl was then added dropwise to the reaction mixture to adjust the pH to ~8, and $NaBH_4$ (60.6 mg, 1.60×10^{-3} mol) was added to the aqueous solution, which was further stirred at room temperature for 1.5 h under N_2. Then, 4 M HCl was added dropwise to the reaction mixture to adjust the pH to 7−8. The EtOH was evaporated, and the remaining aqueous solution was filtered through a cotton plug to remove precipitated salts. The filtered aqueous solution was sealed in a glass vial with a septum and purged with N_2. Cap exchange utilized a biphasic mixture, see Supplementary Figure S1 for a schematic. QDs capped with native hydrophobic ligands (~7.7 nmol in 1.0 mL of $CHCl_3$) were injected by syringe into the aqueous ligand solution with vigorous stirring. The biphasic mixture was stirred at room temperature (or at ~50 °C) overnight under N_2. The $CHCl_3$ layer was discarded after collecting by syringe and the residual $CHCl_3$ in the aqueous layer was removed by evaporation. The aqueous layer was then filtered through a Millex-LCR membrane filter (pore size 0.45 μm, Millipore) and transferred to a centrifugal spin dialyzer (Amicon Ultra 50K, Millipore). The mixture was diluted with DI water and centrifuged at 3400 rpm for 5−10 min, and the clear, filtered solution was discarded. To remove excess unbound ligands and other byproducts, the QD dispersion was subject to a few additional rounds of centrifugation with DI water.

Cap Exchange of Compact Ligands onto Gold Nanoparticles. For cap exchange with AuNPs, the ligands prepared by ester hydrolysis step were used without the subsequent ring-opening reaction of the dithiolane groups due to the much stronger intrinsic Au−S interaction.[28,29] Typical procedures for preparing ligand for cap exchange with AuNPs and the subsequent cap exchange reaction are as follows: LiOH (3.4 mg, 1.4×10^{-4} mol) was added to a mixture of **2** (38.0 mg, 9.42×10^{-5} mol) and DI H_2O (1.0 mL). The reaction mixture was stirred at room temperature for 2 h. Completion of the ester hydrolysis was checked by TLC with $CHCl_3$/MeOH (5:1) as the eluent. Then, 4 M HCl was added dropwise to the reaction mixture to adjust the pH to ~8. Citrate-stabilized AuNPs (5.8 nm diameter, 3.5 mL, 2.8×10^{-10} mol) were added to the ligand solution (in case of ligand 7, 0.1 M NaOH was further added to adjust the pH of the reaction mixture to ~9), and the reaction mixture was stirred at room temperature overnight. The aqueous solution was filtered through a Millex-LCR membrane filter (pore size 0.45 μm, Millipore) and transferred to a centrifugal spin dialyzer (Amicon Ultra 50K, Millipore). The mixture was diluted with DI water and centrifuged at 3200 rpm for 5−10 min, and the clear, filtered solution was discarded. To remove excess unbound ligands and other byproducts, the AuNP dispersion was subject to a few additional rounds of centrifugation with DI water.

Detailed descriptions of the analytical instrumentation, and characterization procedures including pH and salt stability tests; contact angles; protein preparation and labeling; His_n-based self-assembly; agarose gel electrophoresis; EDC coupling; Förster resonance energy transfer (FRET) analysis; along with cell culture procedures including microinjection, imaging QD uptake with cell penetrating peptide, and cytotoxicity test can be found in the Supporting Information.

RESULTS AND DISCUSSION

Design of the Compact Ligands. The primary design criteria for the **CL** series synthesized here was to enhance QD colloidal stability while making overall size significantly smaller, see Figure 1 and Table 1. For inspiration, we drew directly from the properties of peptides and proteins. Their excellent aqueous solubility is partially attributable to the zwitterionic character of their amino acids; that is, the amines and carboxylic acids simultaneously present within most constituent residues can both be ionized.[37,38] Tertiary amine, carboxyl, and hydroxyl groups were chosen as the hydrophilic components to mimic the zwitterionic properties within the ligands. The acid dissociation constant (pK_a) of an alkyl carboxylic acid is ~4.8,[39] which means that it will be mostly deprotonated (ionized) at pHs above the pK_a value. On the other hand, the pK_a of a tertiary amine group is ~10.7[40] and it will be mostly protonated (ionized) at pHs below the pK_a value. If these two functional groups are combined within a single ligand, it is reasonable to expect that the resulting ligand could hold an ionized state over a wide range of pH, though the actual pK_a values in the microenvironments present on QD surfaces may be different from that of the individual group. Alternatively, use of hydroxyl groups is also expected to help aqueous solubility under a wide range of pH because of their strong inherent tendency to form hydrogen bonds with water.[41]

The basic **CL** structure and function continues with a modular design similar to that found in the previous PEGylated ligand derivatives.[24] Ligand−QD interactions are provided by the DHLA's bidentate dithiol motif acting as the first module. This high-affinity attachment is still superior to that of QDs coated with monothiol ligands in aqueous solutions. Rather than depending upon PEG to mediate aqueous solubility in a second module, the new ligands incorporate at least two of the functional groups described above to maintain aqueous solubility in a wide pH range mainly via a zwitterionic character. These groups are purposely designed to serve multiple, simultaneous roles. Besides imparting aqueous solubility under basic pH, the carboxyl groups can be used for further coupling chemistry with biological molecules or organic dyes; this provides a third module or utility to the ligands. The tertiary amino group is expected to enhance aqueous solubility under acidic pH and remain chemically inert to common bioconjugation chemistries such as carbodiimide (e.g., EDC) coupling. Use of the tertiary amine also prevents EDC-based cross-linking (to carboxyls) between the surface ligands on QDs and negates potential issues of cellular toxicity previously noted in the presence of ligands displaying primary amines.[42,43] Four compact ligands were synthesized using these design criteria (Figure 1). **CL1** incorporates two tertiary amines in a piperazine ring structure and terminates in an alkyl carboxyl group. **CL2** includes a single tertiary amine that displays both an alkyl carboxyl and a hydroxyl group. **CL3** is almost identical to **CL2** but ends in two hydroxyl groups. This ligand essentially functions as (i) a control to confirm the necessity of having both a carboxyl and a tertiary amine simultaneously present in the same ligand, and (ii) to verify if the carboxyl group(s) could be substituted with a hydroxyl function. DHLA which represents the non-amine control ligand has already been extensively characterized.[16] **CL4** continues with the same **CL2** and **CL3** motif, but terminates in two alkyl carboxyl groups. The estimated pK_a's of the key ionizable groups on each ligand are given in Table 1. Importantly, **CL1**, **CL2** and **CL4** all display values in both the acidic and basic pH regime matching our key design criteria. In terms of size and mass, **CL1**−**CL4** are estimated to be up to twice the ~1.0 nm extended length of DHLA but less than twice the mass, see Table 1. This contrasts strongly with the

Table 1. Selected Ligand or Quantum Dot Physical Properties

	DHLA	CL1	CL2	CL3	CL4	DHLA-PEG750-OCH_3
Molecular weight	208.34	391.60	366.55	338.54	394.56	926.24 (n = 15)
Synthetic steps	1	4	4	2	4	5
Extended length[a]	~1.0 nm	~2.0 nm	~1.8 nm	~1.6 nm	~1.8 nm	~6.8 nm
pK_a[b]	4.74 (carboxyl)	2.87 (amine)	3.59 (carboxyl)	7.85 (amine)	3.29 (carboxyl)	
Dithiols (10.8/10.2)		4.55 (carboxyl)	8.58 (amine)	14.37 (OH)	3.93 (carboxyl)	
Central amide (16.3)		7.58 (amine)		14.96 (OH)	9.06 (amine)	–
Chemical handle	Yes	Yes	Yes	No	Yes	No
Assembles $(His)_n$ peptide/protein	+/+	+/+	+/+	+/+	+/+	+/–
Contact angles[c]	5°	10°	8°	6°	13°	20°
pH stability range over 4 weeks	7–13 (4 days)	4 (~5)–13	4–13	4–13	5–13	4–11
Zeta potential (mV)[d] at pH 8.3	−20.3 ± 3.9	−39.0 ± 1.9	−19.8 ± 1.6	−4.9 ± 0.8	−50.8 ± 2.7	–
Zeta potential (mV)[d] at pH ~4	–	10.8 ± 0.7	10.3 ± 0.7	22.4 ± 2.1	−19.0 ± 2.2	–
DLS (% Intensity)[e]	10.8 ± 2.70	8.6 ± 1.76	9.3 ± 1.66	9.5 ± 2.10	9.8 ± 2.17	11.5 ± 2.46
DLS (% Volume)[e]	9.2 ± 2.36	7.9 ± 1.82	8.6 ± 1.77	8.6 ± 2.06	8.6 ± 2.08	10.2 ± 2.39
DLS (% Number)[e]	8.1 ± 1.82	7.2 ± 1.62	8.0 ± 1.57	7.8 ± 1.76	7.7 ± 1.76	9.2 ± 2.01

[a] Estimated edge-to-edge molecular length in fully extended structure. [b] pK_a values were calculated by ACD/PhysChem Suite, version 12.01, Advanced Chemistry Development, Inc., Toronto, ON, Canada. [c] Contact angle of water on mica surfaces coated by QDs displaying each ligand. Std. Dev. <10% for all samples. [d] Measured in 1× TBE buffer pH 8.3 and acidified water pH ~4 adjusted with HCl. DHLA-QDs were not measured due to their colloidal instability in the acidic environment. [e] Because of the diverse ways to represent data, the hydrodynamic diameters characterized by different profiles are shown here for comparison. Intensity profile is used for the present discussion.

DHLA-PEG750-OCH_3 sample, which we use frequently[25,44] and which has an estimated geometric length of up to 6.8 nm (~6–7 times longer than that of DHLA) along with a mass ~4.5 times larger than that of DHLA.

Synthesis of Compact Ligands and Cap Exchange in a Biphasic Mixture. An overview of the synthetic procedures utilized to prepare each ligand is shown in Scheme 1. We carefully optimized the reaction conditions and minimized the number of reaction steps. This is an important issue since subsequent QD cap exchange is a mass-driven reaction and requires a large excess of ligand per QD to ensure full overcoating. Synthesis of all the new compact ligands starts from modification of the carboxyl group of thioctic acid (TA) with a primary amine compound. Use of 1,1′-carbonyldiimidazole (CDI) as a coupling reagent is key to the chemistry utilized here as it exclusively gives a primary amine-coupled product in high yield in the presence of a secondary amine group (**1** and **4**).[45] This reaction step significantly simplifies the entire synthetic process by avoiding the need for protecting groups. Subsequent Michael addition reactions of **1**, **4**, and **8** with methyl acrylate formed **2**, **5**, and **9**, respectively. The last steps of the ligand synthetic procedures are (i) deprotection of the methyl ester group to yield the carboxyl group (**2** to **3**, **5** to **6**, and **9** to **10**) and (ii) the ring-opening reduction from a disulfide group to a dithiol group (**3** to **CL1**, **6** to **CL2**, **7** to **CL3** and **10** to **CL4**). Since both of these reactions are simple and quantitative, and each product is highly soluble in water, the reactions were successively performed in aqueous solution. Each ligand required four synthetic preparatory steps except **CL3** which only necessitated two steps. This includes the ring-opening step which is necessary when cap exchanging QDs with all DHLA-based ligands. Importantly, we should note that cap exchange with citrate-stabilized AuNPs can be carried out without the last ring-opening step from TA to DHLA derivatives due to the strong native Au–S interaction (*vide infra*).[28,29] Each synthetic step for **CL1**–**CL4** was straightforward and had a reasonably high yield (≥50% total yields for synthesis of the cap exchange precursors **2**, **5**, **7**, and **9**), clearly fulfilling the desired criteria of facile synthesis of large quantities (gram scale). Final **CL** products were used directly for the cap exchange reaction with QDs coated with the native hydrophobic ligands. All the compounds (**2**, **5**, **7**, **9**) utilized for the subsequent cap exchange were found to be stable for at least 6 months to a year when stored in a refrigerator.

Given the high reaction yield of the ligands and their presence in aqueous solution, we opted to continue working in this media and utilize a biphasic mixture approach[46–48] for cap exchange rather than the single-phase method used previously.[24] The cap exchange reaction was initiated by injecting the hydrophobic QDs dissolved in $CHCl_3$ into the aqueous ligand solution under a N_2 atmosphere with vigorous stirring. As the reaction proceeds, the QDs were gradually transferred from the $CHCl_3$ layer to the aqueous layer in a few hours. The reaction mixture was left with vigorous stirring overnight (Supporting Information, Figure S1). Purified QDs were found to remain bright and be well dispersed in water and colloidally stable over 6 months without any sign of aggregation when stored in a refrigerator (see below).

Characterization of Compact Ligand-Coated Quantum Dots. *Spectroscopic Properties.* We next subjected the aqueous-dispersed **CL**-QDs to a variety of photophysical analyses to characterize the properties the ligands impart to the nanocrystals. Absorption and photoluminescence (PL) spectra were measured for QDs capped with the native hydrophobic ligands in hexane prior to cap-exchange and compared to those functionalized with the **CL**s in H_2O (Supporting Figure S2). The absorption spectra measured before and after cap exchange were essentially unchanged, and occasionally showed only a few nanometers shift of the lowest absorption maxima from batch to batch; PL spectra also showed similar trends. These spectroscopic features are quite similar to our previous QD studies with different DHLA-PEG ligands and indicate that cap exchange with the new **CL** series has no significant optical effect on the inorganic QD core–shell structure.[24,25] It is also quite common to see a decrease in

Scheme 1. Synthetic Schemes for the Compact Ligands Used in This Study: (A) CL1, (B) CL2, (C) CL3, and (D) CL4

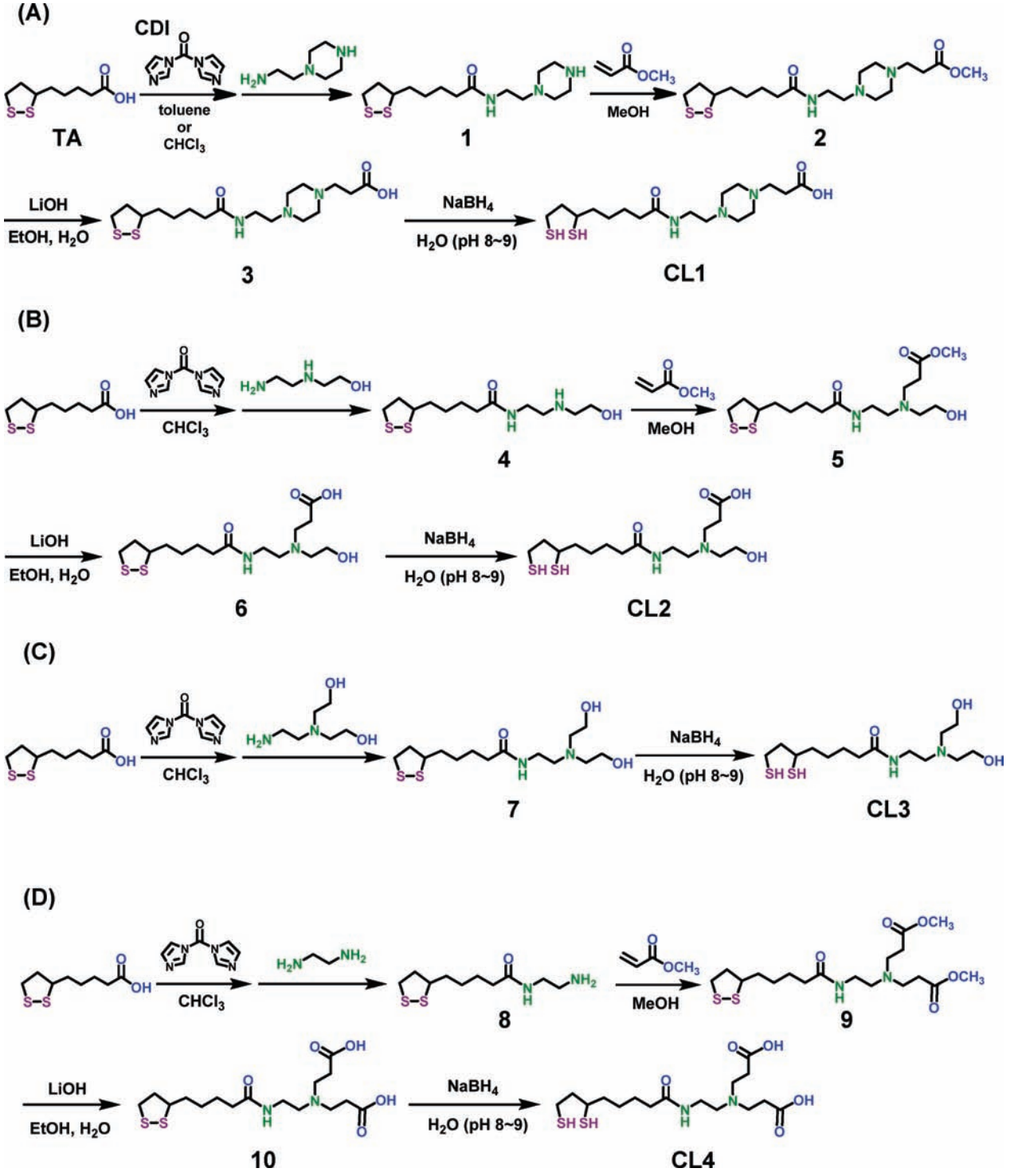

fluorescence quantum yield (QY) of the QD samples following cap exchange and phase-transfer from organic to aqueous media due to incomplete surface passivation and charge effects. Again, similar to our previous reports, we note that the relative QYs after cap exchange dropped to circa half of that measured for the native QD in hydrophobic solvents. QYs for the CdSe-ZnS core−shell QDs used in this study were 25−35% (in hexane) and 10−20% (in water), respectively. As the QD's inherent QY is also a function of the size and integrity of the inorganic shell materials,[46] the CdSe-CdS-CdZnS-ZnS QDs overcoated with several layers of shell materials displaying a gradient of band gap offsets had slightly higher QYs. Following cap exchange and phase-transfer, the QY of these QDs changed from 45−55% (hexane) to 25−40% (water). We note that the Qdot 625 nm emitting ITK

dx.doi.org/10.1021/ja201919s |J. Am. Chem. Soc. 2011, 133, 9480–9496

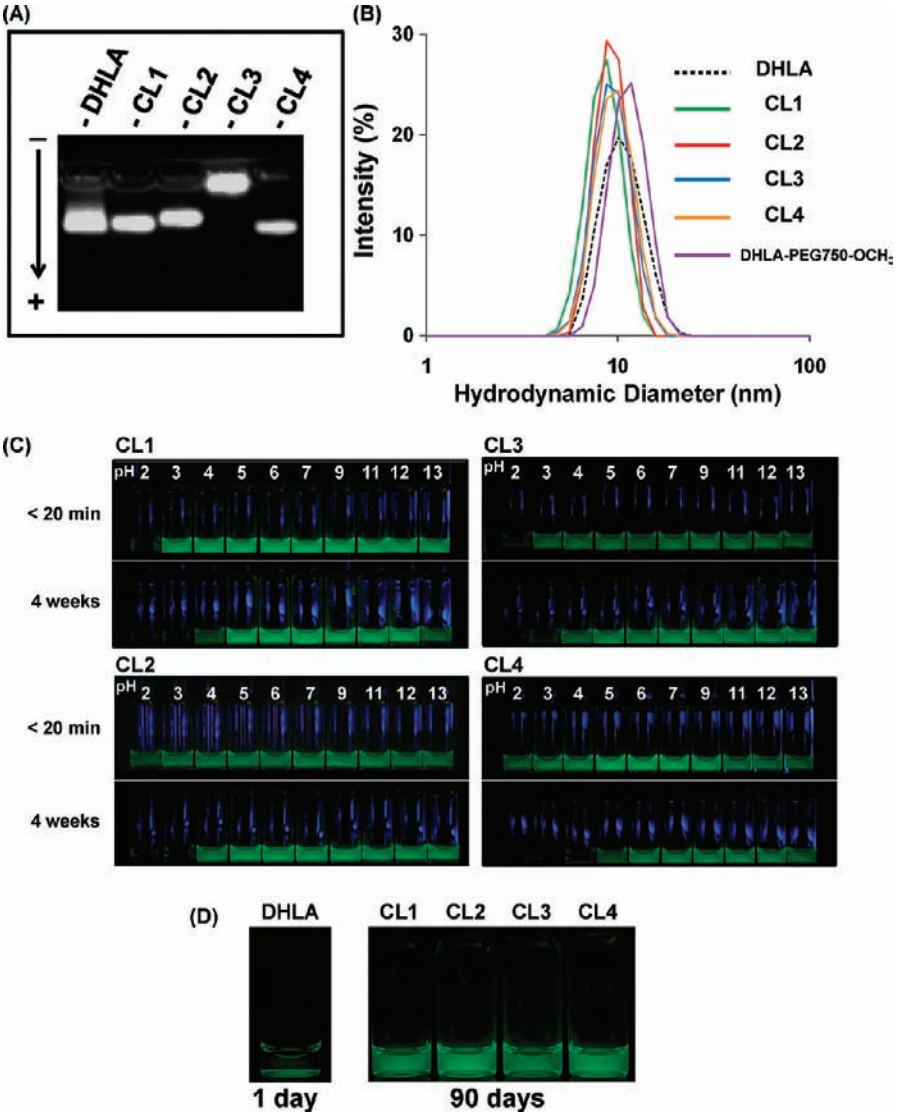

Figure 2. Physical characterization of a series of compact ligand coated QDs. (A) Gel electrophoretic separation of 550 nm emitting QDs cap-exchanged with the indicated ligands. Gels were run on 1% agarose gel in 1× TBE buffer (pH 8.3) at ~7 V/cm for ~10 min. (B) Hydrodynamic size distribution of 550 nm emitting QDs cap-exchanged with DHLA (10.8 ± 2.7 nm), **CL1** (8.6 ± 1.8 nm), **CL2** (9.3 ± 1.7 nm), **CL3** (9.5 ± 2.1 nm), **CL4** (9.8 ± 2.2 nm), and DHLA-PEG750-OCH_3 (11.5 ± 2.5 nm) measured by dynamic light scattering. Data is plotted in arbitrary units of scattering intensity. (C) PL images for a set of 0.5 μM QDs capped with the indicated compact ligands in different buffers at pH 2−13. The 550 nm emitting CdSe-ZnS QDs were used and excited with a UV lamp at 365 nm. Images were taken <20 min and ~4 weeks after sample preparation. (D) PL images for a set of 0.5 μM 550 nm emitting QDs coated with DHLA or the indicated compact ligands in 3 M NaCl solution. Images were taken 1 day after sample preparation for DHLA and 90 days for **CL1**~**CL4**.

QDs (provided by Life Technologies) maintained relatively high QYs after cap exchange: QY was ~78% in hexane and 50−80% in water.

Charge-Based Mobility, Zeta Potential, and Wettability. Hydrophilic QDs cap-exchanged with the **CL** series were also characterized by gel electrophoresis, see Figure 2A. **CL**-QD samples were run together with DHLA-coated QDs in a 1% agarose gel buffered with 1× TBE buffer (pH 8.3). **CL1**- and **CL2**-QDs essentially showed gel mobilities similar to that of the DHLA-QDs. These three ligands are all characterized by having one carboxyl group per ligand which are expected to be exposed on the QD surface, to be ionized at this pH (based on the pK_a values in Table 1), and would then act as the major driving force for electrophoretic mobility in basic buffer. **CL3**-QDs showed only minimal mobility in the electric field. This was expected as **CL3** terminates in hydroxyl groups and not a carboxyl group, and the surface of a **CL3**-QD should, therefore, display an inconsequential net charge in buffer. In contrast, **CL4**-QD presented gel mobility slightly higher than that of the QDs capped with DHLA or **CL1** and **CL2**. The higher mobility in this case is directly attributable to the presence of more negative charges per QD. Since **CL4** terminates in two carboxyl groups, one can expect a higher number of net negative charges present on the QD surface in basic buffer. We also examined the zeta potentials of this series of **CL**-QDs to confirm the gel findings since the solution electrophoretic mobility of NPs should be proportional to the zeta potential.[31] Values for the **CL**-QD samples measured in 1× TBE (pH 8.3) are tabulated in Table 1. We note that the

most negative value is seen for **CL4** (−50.8 mV), followed by **CL1** (−39.0 mV) and **CL2** (−19.8 mV), with **CL3** (−4.9 mV) representing the lowest value. The latter value is quite close to that measured for similar QDs capped with DHLA-PEG molecules which also did not migrate in a gel and displayed an overall neutral character.[31] The minimal mobility of the **CL3**-QDs along with their slight net negative charge in basic buffer is ascribed to the cumulative effect of all the hydroxyl moieties surrounding the QD manifesting a very small pseudo-negative character. Lastly, the higher value for **CL4** in basic buffer is more than double that of **CL2** as expected given the presence of twice the number of carboxyl groups.

We also measured the zeta potentials of the **CL**-QD series in an acidic media of pH ∼4, see Table 1. Positive values of 10.8 and 10.3 mV were obtained for the same **CL1**- and **CL2**-QDs, respectively, at this pH reflecting the balance between protonation of the carboxyl group and ionization of the tertiary amines. The highest value of 22.4 mV was observed for the **CL3**-QDs and reflects the high pK_a of the amine in this construct along with the presence of two hydroxyl groups and no counterbalancing carboxyl groups. Interestingly, **CL4**-QDs displayed a value of −19.0 mV. The negative value in this case reflects the dominating influence of the two appended carboxyl groups functioning in concert and the fact that the surrounding pH is slightly above their pK_a values of 3.29 and 3.93. This is further confirmed by noting that replacing just one of the carboxyl groups with a hydroxyl group yields **CL2** which displays a positive zeta potential at this pH. As expected, control DHLA-QD samples were not colloidally stable in this media and did not allow for reliable measurement. More importantly, the change from a net negative value in basic buffer for **CL1**-, **CL2**-, and **CL3**-QDs to positive values in acidic environment along with the large change in net value for **CL4**-QDs serves as a strong confirmation that the ligands do indeed display the desired zwitterionic properties and, more importantly, can impart them to the QDs. We also note that the microenvironment surrounding the colloidal QD surfaces, which accommodate a very high local concentration of ligands, may have far more complex ionization kinetics than a simple amino acid residue dissolved in a model buffer system.

Some insight into ligand dissolution and interactions within aqueous environments was provided by probing the relative wettability of each ligand. This was accomplished by drying uniform concentrations and volumes of each ligand-coated QD sample onto flat mica surfaces and measuring the subsequent contact angles of water drops using sessile drop goniometry, see Supporting Information. As listed in Table 1, DHLA surfaces produced the smallest contact angle at 5°, while PEGylated QD surfaces produce the largest with a value of 20°. The smaller the observed contact angle, the better the relative interaction of water with a given surface coating. Data for the **CL** series are 10°, 8°, 6°, and 13° for **CL1**, **CL2**, **CL3**, and **CL4** QD surfaces, respectively. The smallest contact angle is obtained for the DHLA-QD and this could be partially attributed to its original presence in basic buffer which was necessary to maintain colloidal stability; electrolytes would enhance the hydrophilicity of the sample. All the other samples were in DI water. Importantly, the contact angles of all the **CL**-QDs were smaller than that of the PEG-coated QDs where far bulkier ethylene oxide repeat units are required for aqueous stability. Indeed we have found that ∼12 ethylene oxide repeats (MW∼600) are usually required for good solubility and wide pH stability.[23] This result suggests that introduction of multiple ionizable groups onto the surface ligands may enhance the hydrophilicity of QD surfaces and help aqueous solubility.

Hydrodynamic Size. We next determined the hydrodynamic diameters for the **CL**-QD series by using dynamic light scattering (DLS) analysis. As shown in Figure 2B and Table 1, the hydrodynamic diameters of the 550 nm emitting QDs coated with **CL1**−**CL4** ranged from 8.6 to 9.8 nm. These values are 1.0−2.2 nm smaller than the 10.8 nm measured for the same materials coated with DHLA and are 1.7−2.9 nm smaller than those functionalized with DHLA-PEG750-OMe (11.5 nm). The hard diameter of the CdSe-ZnS core−shell QD sample used in this analysis was directly measured by TEM to be 4.0 ± 0.29 nm (Supporting Figure S3). The differences in sizes between hydrodynamic diameter and the hard core−shell size measured in all samples arise from hydrodynamic interactions of the ligand layer on the QD surface.[31,46,47] The contribution of the **CL**s to the overall hydrodynamic radius is in the ∼2.3−3.4 nm range, which is reasonably close to that estimated from just the simple fully extended geometric length of each **CL** (1.6−2 nm), see Table 1. The hydrodynamic volume of a colloidal NP is far more complex than this simple extrapolation and is controlled by not only the size and chemical nature of the surface coating materials, but also by the size of the NP itself. Nevertheless, the key feature we note from this analysis is that these new **CL**s provide the functionalized QDs with hydrodynamic volumes comparable to or even smaller than those of DHLA, which is one of the smallest ligands currently utilized for preparing aqueous QDs that are stable over extended time periods in buffer.[16] Moreover, the hydrodynamic size is smaller than that encountered when utilizing far longer PEGylated- or far larger polymer/dendrimer/block copolymer ligands to mediate QD solubility.[31]

Long-Term pH and Salt Stability. We evaluated the long-term colloidal stability of the **CL**-QDs across a wide pH range. The representative images in Figure 2C show the luminescence images of 550 nm emitting QDs coated with **CL1**−**CL4**, respectively, dispersed in buffer solutions increasing from pH 2 up to 13 at time points of 20 min and 4 weeks following sample preparation. Images of the intervening time points can be found in Supporting Figure S4. Strongly acidic conditions (pH 3 or lower) rapidly led to a partial or complete fluorescence quenching and sedimentation of the QDs, similar to the results observed for QDs capped with quadradentate thiol ligands at the same pH.[49] We surmise that this strongly acidic environment results in reactive 'acidic' etching of the nanocrystal or destabilizes the ligand-QD bonds. The remaining QD dispersions were colloidally stable in weakly acidic to strongly basic pH conditions (pH 4−5 to 12−13) without apparent fluorescence quenching for at least a 2 month period. **CL**-QDs were also found to be stable in DI water for at least 6 months. This excellent pH stability directly contrasts with that observed for DHLA-coated QDs. While colloidally stable in basic media, DHLA-coated QDs became unstable even in weakly acidic media in a few days (Supporting Figure S5). We note that the pH stability of the present **CL**-QDs is comparable to that of QDs coated with DHLA-PEG ligands where the lengthy and neutral ethylene oxide repeat units mediate aqueous solubility.[24,25] We attribute this to their zwitterionic nature of **CL1**, **2** and **4** which display pK_a's in both the acidic and basic regime and thus should be ionized across a broad pH range. Interestingly, this also suggests that the two hydroxyl groups on **CL3** are also capable of at least contributing to aqueous solubility when presented in conjunction with a tertiary amine. The colloidal stability of the **CL**-QD series was also

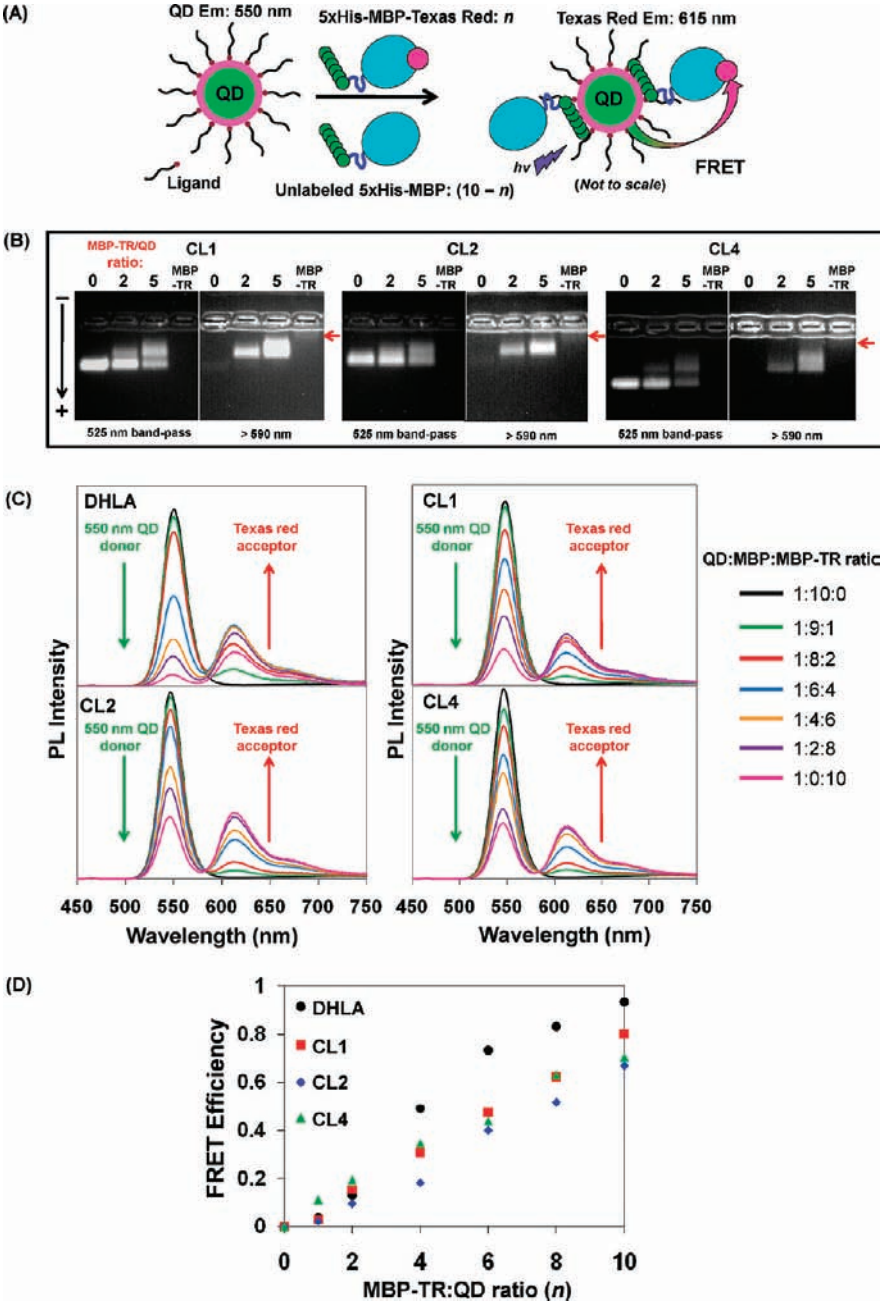

Figure 3. His-tagged MBP-QD interactions and FRET. (A) Schematic of the FRET assay used to investigate direct assembly of His-tagged MBP labeled with Texas Red onto QD surfaces. For electrophoresis, QDs were assembled with His-tagged MBP-Texas Red only, while for FRET, a mixture of His-tagged MBP and His-tagged MBP-Texas Red was used. (B) Gel electrophoresis separation of 550 nm emitting **CL1**-, **CL2**-, and **CL4**-QDs self-assembled with "*n*" equivalents of His-tagged MBP-Texas Red. Lane labeled '0' contains only QD while that labeled 'MBP-TR' contains only His-MBP-Texas Red. Bands corresponding to free MBP-TR are indicated with red arrows. Gels were run on 1.5% agarose gel in 1× TBE buffer (pH 8.3) at ~10 V/cm for ~10 min and imaged with 525 nm band-pass or 590 nm long-pass filters to highlight the QD and Texas Red fluorescence components, respectively. (C) PL spectral changes from 550 nm emitting DHLA-QD and **CL**-QDs titrated with a mixture of "*n*" equivalents of 5×His-tagged MBP-Texas Red and "10-*n*" equivalents of 5×His-tagged MBP (unlabeled). The total number of His-tagged proteins per QD was fixed as 10 while the discrete ratio of dye-labeled MBP per QD was varied systematically. (D) FRET efficiencies from DHLA-, **CL1**-, **CL2**-, and **CL4**-QDs in (C) as a function of MBP-TR/QD ratio (*n*).

examined under high salt concentration (Figure 2D). Each QD was dispersed in 3 M NaCl solutions (pH ~6) and monitored over time. Again DHLA-coated QDs precipitated within a day at this salt concentration while all the **CL**-QDs appeared stable and well dispersed for at least 3 months. The generally accepted relevant physiological NaCl concentration is ~150 mM,[50] and biological environments are also known to be rich in a variety of other strong electrolytes. This strongly suggests that **CL**-coated QDs may be quite tolerant of similar ion-rich biological environments for long time periods.

Assembly of His-Tagged Proteins and Förster Resonance Energy Transfer. Recombinantly modifying proteins to express

oligohistidine tags (His_n) was originally implemented to facilitate their large-scale, efficient purification with metal-affinity chromatography.[51,52] In recent years, we, along with a growing number of other groups, have utilized these same metal-affinity interactions to conjugate CdSe-ZnS QDs to an array of oligohistidine-appended proteins, peptides, and even appropriately modified DNA to assemble a variety of QD bioconjugates for sensing, imaging, and cellular probing applications.[17−21,48,53−57] His_n-interactions arise from collective metal-affinity coordination between the pendant imidazolium side-chains of histidine residues and the Zn-rich surface of QDs.[18] Inherent benefits provided by this simple but effective QD-bioconjugation approach include: (i) ease of use as it is based completely on self-assembly and only requires mixing of the two reagents; (ii) rapid self-assembly with an intrinsically high affinity ($K_d \sim 1$ nM); (iii) control over the valence of His_n-biomolecules attached per QD through the molar ratios used; (iv) direct use of His_n-QD bioconjugates in subsequent assays without requiring further purification; (v) control over biomolecular orientation on the QD; (vi) application to QDs coated with a number of different surfaces/ligands; and (vii) due to their small size, His_n-modifications have only minimal effects on the tertiary structure and biological activity of the proteins and peptides to which they are appended.

Given the growing popularity of His_n-QD bioconjugation, it was important to evaluate whether similar assembly could be achieved with the **CL**-QD series. Previous studies revealed that, although smaller peptides can interact with many types of QDs via His_n-interaction, conjugation to proteins in the same manner required the use of QDs capped with short DHLA surface ligands.[18,20,21,23] When attempting to use PEGylated QDs as His_n-substrates, the larger, globular nature of proteins combined with the steric hindrance of the long PEG chains on the QD surface prevents the His-tag from interacting directly with the metal-rich QD surface. However, as DHLA-capped QDs are stable only in basic buffers, this has severely limited effective use of DHLA-QD/His_n−protein conjugates. Clearly, significant minimization of the steric hindrance caused by the surface ligands on the QDs is a prerequisite to ensure a stable conjugation between QDs and His-tagged proteins. The **CL** series are expected to increase the chance that His_n-tags on proteins reach the QD surface and form stable binding interactions with it.

The capability of direct His_n-tagged protein conjugation onto **CL**-QD surfaces was examined in two ways: agarose gel electrophoretic separation and FRET analysis. As a test protein, we utilize the *Escherichia coli* periplasmic maltose binding protein (MBP). This medium sized protein (∼44 kDa) has dimensions of 30 × 40 × 65 Å with a volume of ∼78 × 10^3 $Å^3$ and has found strong utility as a test platform in biosensing.[58] MBP displaying a C-terminal pentahistidine sequence was site-specifically labeled on residue 95C with Texas Red maleimide dye (5xHis MBP-TR) as described in the Supporting Information. For gel electrophoretic analysis, dye-labeled MBP alone was self-assembled to 550 nm emitting QDs capped with **CL1**, **CL2**, and **CL4** at ratios of 0, 2, and 5 per QD (see Figure 3A for schematic). As **CL3** is neutral and is not expected to show sizable gel mobility, it was not tested in this configuration. QD-MBP-TR conjugates were then separated side-by-side with free MBP-TR in 1.5% agarose gels where use of different filters allowed separate visualization of the QD and sensitized Texas Red emission bands on the gel using UV excitation.[59] Figure 3B shows that as the ratio of 5×His MBP-TR was increased, discrete slower moving bands appeared along with the higher mobility unconjugated QD bands for each of the **CL**-QD samples when observed with the 525 nm band-pass filter. The unconjugated QD front-moving band also visibly decreases in intensity with increasing MBP-TR. The Texas Red bands visualized with the 590 nm long-pass filter coincide with those of the slower moving QD/MBP-TR conjugates. Changes in mobility of QD/MBP-TR conjugates are due to increases in relative mass/charge arising from assembly of MBP-TR onto the QD surface. In comparison, the slowest gel mobility was observed for unconjugated MBP-TR which also appears quite faint due to a low direct and unsensitized excitation in the UV. Colocalization of the QD and Texas Red emission, along with sensitization of the latter for co-assembled samples, confirm that the QDs and MBP-TR are indeed conjugated and migrating together.

Since the PL of 550 nm emitting QD and the absorption of Texas Red have a sizable spectral overlap (I of 2.98 × 10^{-13} M^{-1} cm^3 and R_0 of 45 Å, see Supporting Figure S6), formation of the QD-MBP-TR conjugates was expected to facilitate an efficient level of energy transfer from the QD donor to the proximal Texas Red dye acceptor. For evaluating **CL**-QD intraconjugate FRET, we utilize a slight modification during the self-assembly process. It has been previously demonstrated that conjugation of His-tagged biomolecules onto QD surfaces commonly increases the fluorescence intensity or QY of the QDs; this enhancement is ascribed to protein passivation of surface trap states on the QD surface.[60,61] Assembling unlabeled 5×His MBP onto the current **CL**-QD series resulted in similar changes further confirming His-tagged MBP binding to **CL**-functionalized nanocrystals, see Supporting Figure S7 for a representative example. To effectively address PL enhancement caused by His-tagged protein binding onto QDs during the subsequent FRET analysis, the total amount of His-tag MBPs assembled was fixed at 10 equiv per QD, while the discrete ratio of Texas Red-labeled (n) and unlabeled His-MBP (10-n) was systematically varied (n = 0−10) as shown in Figure 3A. This approach has been utilized previously,[60,61] and mitigates issues of changes in PL enhancement and the need for a more complex analysis to account for self-assembly heterogeneity at low ratios.[62]

Figure 3C shows a series of representative fluorescence spectra collected from dispersions of the same **CL**-QD series as above incubated with MBP-TR at increasing ratios and excited at 400 nm where the absorption of Texas Red is minimized. DHLA-coated QDs were also measured as a positive control sample. As MBP-TR ratios increased, each QD/MBP-TR conjugate showed a decrease in QD PL concomitant with the appearance of a new fluorescence band at ∼615 nm arising from Texas Red sensitization. The trends in these data sets closely mirrors that previously collected from a series of DHLA-capped QDs assembled with MBP labeled with Cy3-acceptor in the same 95C position.[61] Increases in FRET efficiency within each conjugate extracted from the decrease of QD donor PL versus assembly valence are plotted in Figure 3D. Analysis of this data using Förster formalism and eqs 1−3 in the Supporting Information derived QD-donor to dye-acceptor separation distances r of 65 ± 7 Å (DHLA-QDs), 65 ± 5 Å (**CL1**-QDs), 73 ± 6 Å (**CL2**-QDs), 64 ± 3 Å (**CL4**-QDs). The fluorescence enhancement of the QDs following assembly with 10 equiv of His-tagged MBPs (Figure S7) was measured, and the increased QYs of the QD-MBP conjugates were accounted for within each sample configuration in this analysis. Interestingly, the averaged r values for the

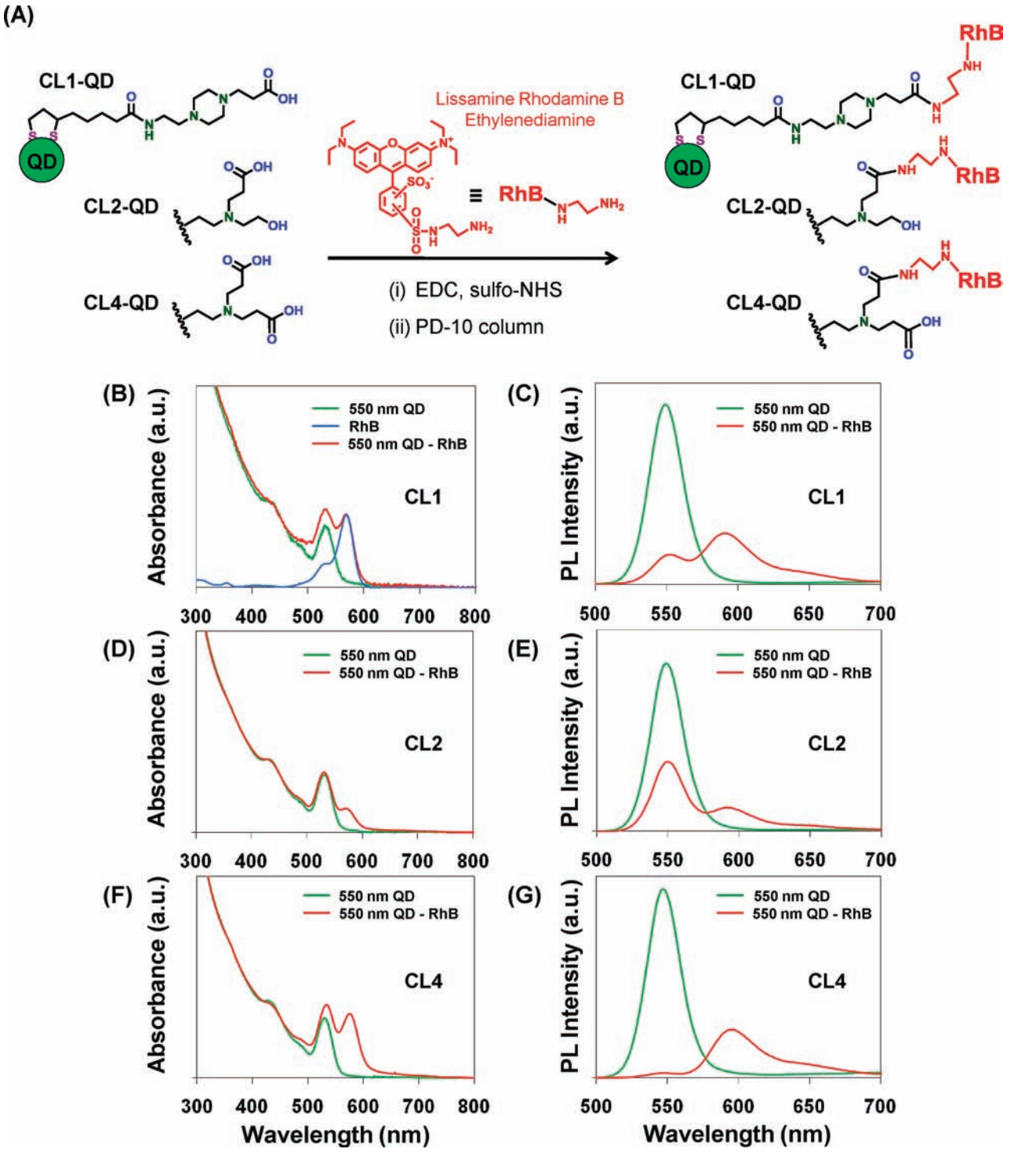

Figure 4. EDC coupling chemistry. (A) Schematic representation of EDC coupling of **CL**-QDs with Lissamine rhodamine B ethylenediamine. Only one of the two available carboxyl groups on **CL4** is shown modified. Respective absorption and PL spectra of the first eluting band following gel filtration of reaction mixtures of 550 nm emitting QDs and Lissamine rhodamine B ethylenediamine for (B and C) **CL1**-QDs; (D and E) **CL2**-QDs; and (F and G) **CL4**-QDs versus QD samples in the control reactions lacking EDC. The 15-fold excess dyes per QD were used for each reaction. In panel B, the native absorption spectrum of Lissamine rhodamine B ethylenediamine is also shown as blue line. PL spectra were measured using either 400 or 440 nm excitation.

CL-QD series are similar to those determined with the DHLA-QDs, suggesting that **CL** series are still small enough to provide close proximity between the QD donor and acceptors; this was also suggested by the DLS data. Slightly higher FRET efficiency of DHLA-QDs compared with the **CL**-QD series is due to the higher fluorescence enhancement of DHLA-QD observed when assembled with His-tagged MBP (data not shown). We also surmise that the actual number of His-tagged MBP bound on

dx.doi.org/10.1021/ja201919s |*J. Am. Chem. Soc.* 2011, 133, 9480–9496

CL-QDs could be lower than that of DHLA-QDs due to the slightly bulkier structures of the **CL** series compared with DHLA. Different ligand structures and packing may also sterically alter MBP orientation, which may concomitantly affect location of the acceptor dye and FRET efficiency. We note that His-tagged TR-labeled peptides could also self-assemble on the **CL**-QD series and engage in efficient FRET (see representative example in Supporting Figure S8). This was not surprising given that His-tagged peptides are usually >10-fold smaller than His-tagged proteins and can even access the surface of PEGylated QDs. Overall, it is clear that the present **CL** series are small enough to allow direct His-tag mediated conjugation of proteins onto the QD surface. The ability to directly conjugate QDs with His-tagged proteins and peptides in a simple manner with good control over the resulting hybrid architecture will contribute to wider utility and allow for more sophisticated QD-bioconjugate design.[14,15]

Chemical Conjugation to Compact Ligand Functionalized Quantum Dots. The ubiquitous presence of carboxyl and amine groups on proteins and peptides along with their easy introduction onto QDs and other NPs has made carbodiimide (e.g., EDC) chemistry perhaps the most popular method for attaching biological moieties to QDs.[4,9,15,24,41] To verify that the terminal carboxyl groups of **CL1**, **CL2**, and **CL4**, when present on the QD surface, are available not only for aqueous solubility but also for chemical conjugation with other molecules, aqueous EDC coupling reactions were carried out with an amine-terminated dye. Since the 550 nm emitting QDs used here and Lissamine rhodamine B ethylenediamine dye (Life Technologies) have significant spectral overlap (I of 5.3×10^{-13} M^{-1} cm^3 and R_0 of 49 Å, see Supporting Figure S9), EDC coupling between the QDs and this dye is expected to place them close enough to allow efficient FRET from the QD donor to the dye functioning as acceptor. QDs coated with either **CL1**, **CL2**, or **CL4** were mixed with 15-fold excess dye along with EDC and sulfo-NHS in 10 mM phosphate buffer pH 7.0 or PBS buffer as described in the Supporting Information (Figure 4A). The reaction mixture was stirred for ~2 h at room temperature and directly passed through PD-10 gel filtration columns (GE Healthcare, Inc.) to remove the reagents and unbound dyes. The same reactions without EDC were carried out as controls to examine potential nonspecific adsorption of the dyes onto the QD surfaces. The first fluorescent fraction eluting from the columns was collected and used in the subsequent spectroscopic measurements. Figure 4B−G shows the absorption and PL spectra of this first eluent from the reaction mixtures superimposed over that collected from control reactions without EDC. For comparison purposes, Figure 4B also plots the absorption of rhodamine dye. The absorption spectrum collected from each EDC reaction (Figure 4B,D,F) is characterized by the presence of a new peak around 570 nm originating from the rhodamine dye together with the QDs lowest absorption band around 530 nm. Absorption spectra of the same fraction collected from control reactions without EDC were identical to those of the original QD sample.

The average number of conjugated rhodamine dyes per QD was estimated to be ~2.0, ~0.7, and ~1.9 for the **CL1**, **CL2**, and **CL4** samples, respectively, by assuming that the absorption spectrum of the QD-dye conjugate is the sum of the individual spectra of QD and dye. The coupling efficiency of **CL2**-QD was smaller than that of **CL1**-QD and **CL4**-QD and we found that using a higher dye/QD ratio for the EDC coupling increased the number of the conjugated dye per **CL2**-QD (data not shown). PL spectra of the QD-dye conjugates (Figure 4C,E,G) showed a significant decrease of the original QD fluorescence along with increase of the dye fluorescence. Since the conjugates were excited at either 400 or 440 nm where the absorption of the rhodamine dye is negligible, fluorescence enhancement arises mostly from FRET sensitization. The FRET efficiency of the QD-dye conjugates was ~84%, ~58%, and ~97% for the respective **CL1**, **CL2**, and **CL4** samples as calculated from QD donor PL changes before and after dye conjugation. These spectral features indicate that (i) EDC coupling worked to covalently couple the carboxyl group of the compact ligands on the QD surface to the amine group of the rhodamine dye, and (ii) the standard reaction condition used here did not cause any significant nonspecific adsorption between the QDs and dye. We also did not observe any visible aggregation or precipitation during the reactions and the following purification step. Though the coupling conditions were not fully optimized, the present data set clearly demonstrates that the carboxylic acid groups of **CL**s are available for further chemical conjugation. This result is important in light of several reports indicating that carboxyl groups may have a high propensity to directly interact with QD surfaces.[10,63]

Cellular Delivery of Compact Ligand-Coated Quantum Dots. One of the fastest growing areas of QD utility continues to be that of cellular labeling and imaging. Among the continuing issues related to this are access to facile methods for delivering the QDs to the cells and the effects on subsequent cellular viability.[5,64] We examined delivery of the **CL**-QD series to cells and monitored their subsequent intracellular stability using both active microinjection and the more passive technique of peptide-facilitated uptake.

Microinjection. Adherent COS-1 cells grown in coverslip-bottom plastic dishes were microinjected with 2 μM of each **CL**-QD diluted into 1× PBS. The cells were then repeatedly imaged by epifluorescence microscopy over a 6 h period to follow the intracellular PL distribution of the QDs. This technique allows us to directly access the cytosol and probe the *in vivo* colloidal stability of the **CL**-QDs. The 550 nm emitting QDs were used with **CL1** and **CL2**, while 625 nm emitting ITK QDs were utilized with **CL4**. As can be seen in the representative time-lapse image set shown in Figure 5A, PL from the QDs maintained a strong level of signal inside the cells and an almost uniform staining pattern. Further, in almost all cells examined, the QDs were located throughout the cytosol but were clearly excluded from the nuclei. These results clearly indicate that the **CL**-QDs were well dispersed in the cytosol without aggregation. Although addressing of individual cells by this technique does not allow for full assessments of toxicity/viability, cells appeared to be intact and visibly unperturbed for at least 6 h following injection. This suggests the availability of an experimental window for more complicated intracellular sensing experiments using this delivery mechanism with probes assembled around these types of materials. The excellent colloidal stability of these **CL**-QDs in the cellular environment is in marked contrast to DHLA-QDs, which exhibited punctate fluorescence under similar conditions, suggesting rapid aggregate formation and precipitation.[23] Repeated attempts to microinject **CL3**-QDs failed with the nanocrystal samples appearing to precipitate at the cell-microinjector tip interface. The reasons behind this are not readily apparent given the good pH and salt-stability observed above for QDs capped with this ligand (*vide supra*).

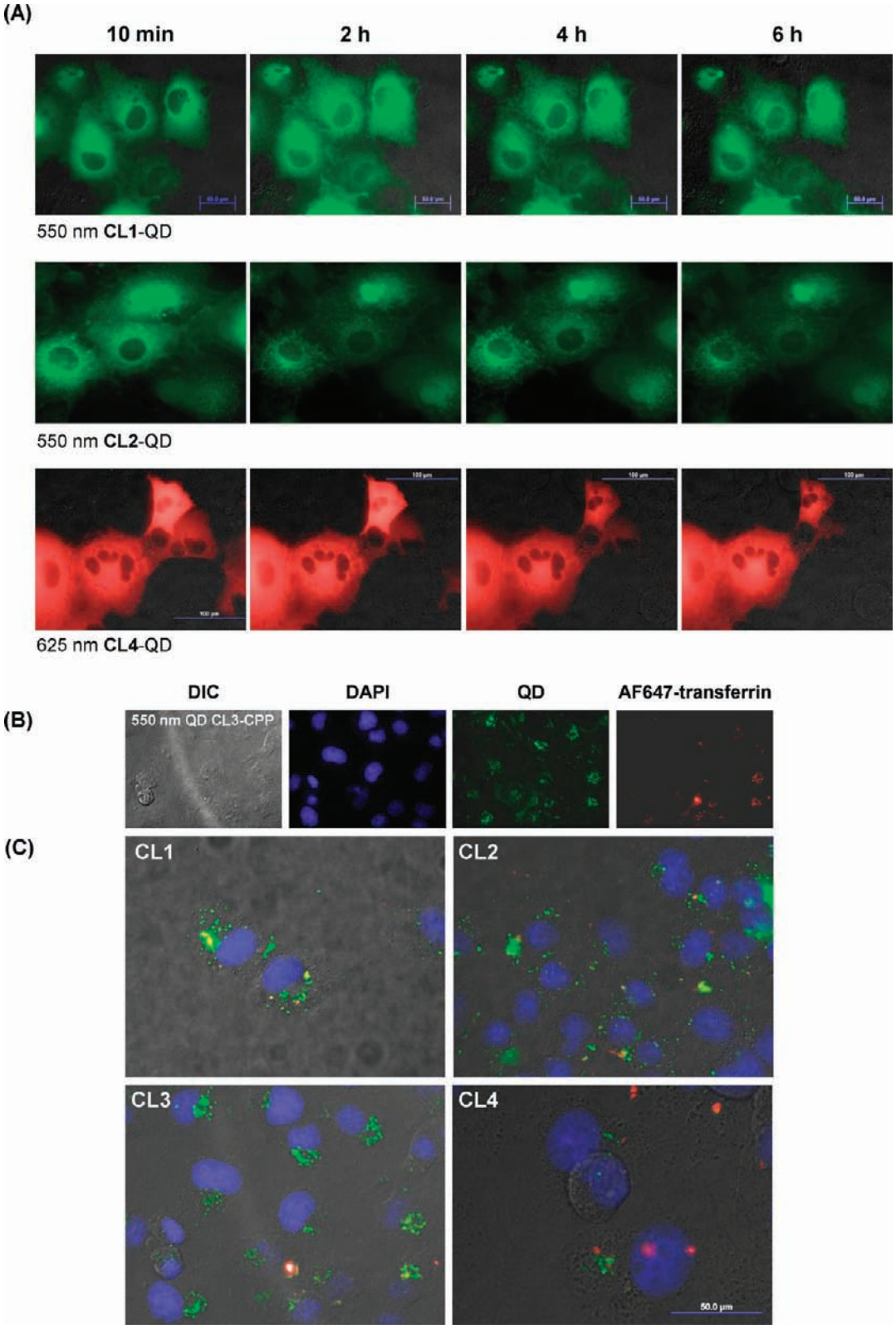

Figure 5. Cellular delivery. (A) Representative epifluorescent images of COS-1 cells at different time periods following microinjection with 550 nm emitting **CL1**-QD, 550 nm emitting **CL2**-QD, and 625 nm emitting **CL4**-QD. The **CL**-QDs were injected directly into the cytosol of the cells. (B) Images corresponding to the differential interference contrast (DIC), DAPI, 550 nm emitting QD, and AlexaFluor647-transferrin fluorescence for COS-1 cells exposed to **CL3**-QD-CPP assemblies. (C) Merged images for cells exposed to assemblies of the **CL**-QD series with CPP. COS-1 cells were co-incubated with 550 nm emitting **CL**-QD-CPP assemblies (**CL**-QD/CPP ratio 1:25) at QD concentrations of 100 nM and 30 μg/mL AlexaFluor647-transferrin for 1−2 h. The nuclei were counterstained with DAPI following fixation.

dx.doi.org/10.1021/ja201919s |*J. Am. Chem. Soc.* 2011, 133, 9480–9496

Cellular Uptake of Compact Ligand Coated Quantum Dots Self-Assembled with Cell Penetrating Peptide. As an alternate to the microinjection format described above, we also assessed whether the **CL**-QD series could undergo peptide-facilitated delivery to the same cells. The cell penetrating peptide (CPP = R_9GGLA(Aib)SGWKH_6) used in this study is composed of two functional sequences separated by a GGLA(Aib)SGWK linker. The C-terminal oligohistidine sequence allows the peptide to self-assemble onto the QD surface via metal-affinity interactions, while the N-terminal oligoarginine sequence allows specific QD delivery across the cellular membrane.[57,64,65] Use of canonical polyarginine peptidyl motifs, originally derived from the HIV transcriptional activator or Tat protein, has facilitated endocytic uptake of a number of different cargos including QDs and other NPs into cells. Mechanistically, it is believed that their inherently strongly positive charge interacts with the negatively charged heparan sulfate proteoglycan receptors present on the cellular membrane prior to endocytosis and membrane turnover.[64−66]

COS-1 cells were incubated for 1−2 h with either **CL**-QD-CPP assembled at 25 or 50 equiv of CPP per QD or control nonconjugated **CL**-QDs. The representative epifluorescent images in Figure 5B,C show that self-assembly of CPP across the entire **CL**-QD series results in efficient cellular uptake of the conjugates. The complete image set is shown in Supporting Figure S10. Punctate QD fluorescence was observed throughout the cytoplasm as well as in close proximity to the cell nuclei counterstained with DAPI. However, no nuclear staining by the QDs was apparent. Furthermore, we observed no detectable fluorescence signal remaining on the plasma membrane, indicating a negligible degree of nonspecific binding of **CL**-QD-CPP assemblies to the cells after washing. **CL**-QDs without CPP also showed only negligible intracellular fluorescence and nonspecific binding on the plasma membrane after washing (Supporting Figure S11). In contrast to the microinjection results, **CL3**-QD-CPP assemblies demonstrated very efficient delivery to the cells. The punctate nature of endosomal QD staining does not, however, allow us to determine whether they remain dispersed or aggregated in this acidic cellular compartment. These results confirm that self-assembly of CPP with **CL**-QDs allowed for specific cellular internalization. The fate of the internalized **CL**-QD-CPP assemblies were confirmed by simultaneous delivery of the endosomal marker AlexaFluor 647-labeled transferrin (AF647-transferrin), which is commonly used to monitor the endocytic pathway.[57] The merged fluorescent images in Figure 5C showed that a significant portion of the internalized QD-CPP assemblies were colocalized with AF647-transferrin confirming that the **CL**-QD-CPP assemblies were mostly distributed within endosomes and intracellular delivery of the assemblies was driven by endocytotic uptake. We have observed similar CPP-mediated endocytic internalization for both DHLA and PEGylated QDs.[57,67] The primarily perinuclear localization of the **CL**-QD-CPP assemblies is also in keeping with previous results and is believed to occur as the vesicles transition to late endosomes within the endolysosomal system.[57]

Cytotoxicity. Lastly, we examined the potential toxicity of delivering **CL**-QDs to cells using a colorimetric tetrazolium-based cell proliferation assay which monitors the inhibition of cellular proliferation.[57,67] Equivalent concentration ranges of **CL**-QD-CPP assemblies, unconjugated **CL**-QDs, and free CPP were exposed to the COS-1 cells using the same conditions as above. Following washing steps and a subsequent 72 h culture, no detrimental changes in proliferation for the CPP (tested up to 6.2 μM), unconjugated **CL**-QDs (tested up to 200 nM), or **CL**-QD-CPP assemblies (CPP/**CL**-QD ratio of 25:1, **CL**-QD tested up to 200 nM) relative to the untreated control were observed (Figure 6). Interestingly, **CL4**-QD-CPP assemblies appear to have a mildly stimulative effect on the cells in this assay format, similar to the results reported for exposing mouse immune cells to mercaptopropanoic acid-capped QDs.[68] We note that this is the same exposure time utilized to achieve the CPP-mediated cellular delivery above and that this regime has also been shown to be nontoxic for delivery of other types of DHLA and PEGylated QDs to various cell lines.[57,67]

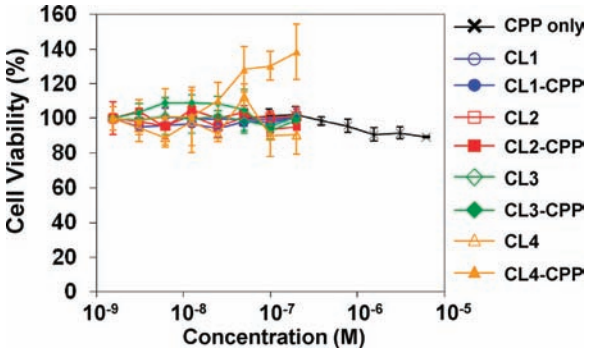

Figure 6. Cytotoxicity assay results demonstrating the effects of CPP, **CL**-QDs, and **CL**-QD-CPP (QD/CPP ratio = 1:25) assemblies on cellular proliferation of COS-1 cells. COS-1 cells were incubated with the materials for 2 h, washed, and subsequently cultured for 72 h prior to the viability assay. Each data point represents the mean ± standard deviation of triplicate measurements.

Compact Ligand-Functionalization of Gold Nanoparticles. To demonstrate that the **CL** series could be useful for solubilizing other NP materials beyond QDs, we also tested their applicability with AuNPs. While single thiol-appended zwitterionic ligands including cysteine and glutathione have been widely applied to AuNPs due to the stable Au−S interactions,[69−72] use of these dithiol ligands with zwitterionic character can further enhance the colloidal stability and thus has some benefits for long-term use in biological studies under harsh conditions compared with single thiol analogues.[28,29] In contrast to the coating procedure used with the QDs, surface functionalization here does not require a reduction step to open the dithiolane ring, rather the thioctic amide derivatives of **CL**s (**3**, **6**, **7**, **10**) are added in excess to citrate-stabilized AuNPs and the inherent gold−sulfur interactions open the dithiols during cap-exchange.[28,29,73] Citrate-stabilized 5.8 nm AuNPs were cap-exchanged with the **CL** series along with DHLA as described in the Materials and Methods. The **CL**-AuNPs were then subjected to a battery of the same characterization tests as the **CL**-QD series. Gel electrophoresis was used to verify that the ligands would impart similar surface charge/mobility characteristics to the AuNPs. As can be seen in Figure 7A, the **CL**-AuNPs have an almost identical gel migration pattern as **CL**-QDs when compared to DHLA-AuNPs (compare Figure 7A to Figure 2A) suggesting that almost the same relative surface-charge properties are imparted to these materials. Results of the DLS analysis can be found in Supporting Figure S12. The hydrodynamic diameters of the 5.8 nm AuNPs coated with **CL1**−**CL4** ranged from 12.1 to 13.9 nm. These values are comparable within error to the 13.2 nm measured for the same AuNPs coated with DHLA and are again much smaller than those functionalized with

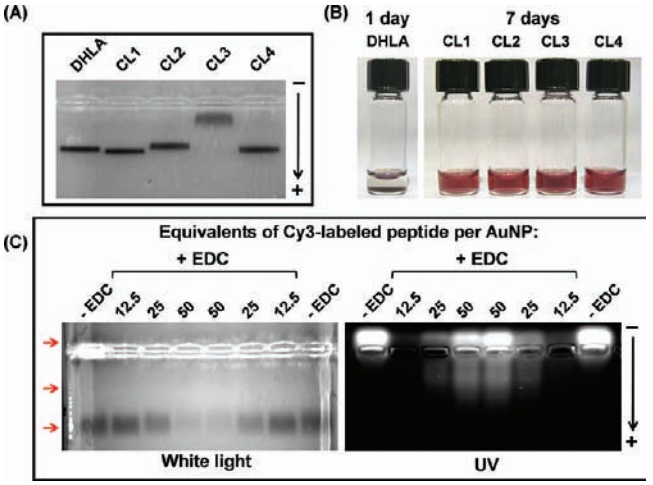

Figure 7. Compact ligand coated gold nanoparticles. (A) Gel electrophoresis separation of 5.8 nm AuNPs cap-exchanged with the indicated ligands. Gels were run on 1.5% agarose gel in 1× TBE buffer (pH 8.3) at ~10 V/cm for ~10 min. (B) Images of 200 nM DHLA and **CL**-AuNPs suspended in 2 M NaCl. Images were taken 1 day after the sample preparation for the DHLA sample and 7 days for the **CL1**~**CL4** samples. (C) Gel electrophoresis separation of **CL4**-AuNPs EDC-coupled to a Cy3-labeled peptide displaying a single, internal lysine amine. The numbers indicate the equivalents of labeled peptide present in each reaction run in that lane. '-EDC' correspond to control AuNP samples incubated with 50-fold excess of peptide in the absence of EDC. Gels were imaged with both white light and UV illumination. Red arrows (from top to bottom) indicate the presence of unreacted peptide, AuNP/peptide conjugates and AuNPs.

DHLA-PEG750-COOH (17.3 nm). These trends are quite similar to the results collected from the QDs above. We found that the **CL**s also provided the AuNPs with a similar colloidal stability over time, see Figure 7B.

To verify that the carboxyl groups on the **CL** series would also be available for subsequent chemical modification, we performed EDC coupling reactions with a Cy3 dye-labeled peptide that had a unique lysine-amine within its sequence, see Supporting Information. Figure 7C shows representative data where **CL4**-AuNPs were reacted with increasing concentrations of excess dye-labeled peptide and then separated on a 1.5% agarose gel. As can be seen under white light illumination, the conjugated AuNPs undergo a small decrease in migration relative to control samples with no EDC present plus 50-fold excess of peptide, see the corresponding lanes indicated with '-EDC'. Mobility shifts directly track the increased ratios of labeled peptide present in the reactions along with a concomitant decrease in the intensity of the fast-moving unconjugated AuNP band. Under UV illumination, unconjugated peptide is visualized migrating in the opposite direction coinciding with its very slight positive charge at the buffer pH of 8.3. Fluorescence is also observed between the fast-moving AuNP band and the loading wells of the gel, and the relative emission here increases concomitant with the ratio of peptide present in the reaction. This fluorescence arises from the peptide that is EDC-conjugated to the AuNPs and its largely diffuse migration corresponds to the heterogeneous valence of labeled product as expected. Very little emission is seen in lanes corresponding to the 12.5 ratio of excess peptide used; this was also expected given both a low predicted peptide attachment and strong dye quenching from the gold.[73] Although only an initial overview, these results clearly confirm that **CL** properties can be extended to other NPs beyond QDs.

CONCLUSIONS

The concept of designing QD ligands to be both compact and simultaneously zwitterionic has been attempted before. Bawendi's group utilized the amino acid cysteine with CdSe-CdZnS core−shell QDs which allowed it to function as one of the smallest QD ligands known after mercaptoacetic acid, along with providing a zwitterionic character.[46] Use of this natural residue as a ligand, however, resulted in materials that were stable for ~24 h without adding the additional presence of a strong reducing agent; a result attributed to ligand dissociation and subsequent oxidation which formed cystine dimers that did not reaccess the nanocrystal surface. The cysteine analogue penicillamine[74] and the tripeptide glutathione[75,76] have also been used as ligands with the intent of providing similar zwitterionic properties to QDs.[10] Muro et al. reported a QD ligand that is somewhat closer in design to our **CL** series.[47] Here, DHLA was used in a similar manner to provide high affinity with the QD surface while the zwitterionic nature was provided by an appended sulfobetaine group. Kim recently synthesized a ligand analogous in concept to that of Muro where DHLA was also linked to a sulfobetaine group.[77] QDs capped with the latter ligands and control ligands were utilized for a series of cellular studies.[77] It is important to note that the quaternary amine and sulfonate groups in both Kim's and Muro's design precluded further chemical conjugation which could only be provided to those QDs by creating a mixed nanoparticle surface displaying several *different* functionalized ligands.

We report here the design and synthesis of a series of new DHLA-based compact ligands which allow preparation of robust and biocompatible QDs for biosensing and cellular imaging applications. The structures of these new DHLA-based ligands are simple and they are easily synthesized in large quantities from available materials in four-steps that include ring-opening. Inherent benefits that these ligands provide for biological applications include: (i) high-affinity interactions with the QD surface; (ii) small hydrodynamic size of QDs, comparable to that of DHLA-QDs; (iii) enhanced colloidal stability under a wide pH range and high salt concentration; (iv) direct conjugation of His-tagged proteins and peptides onto QD surfaces; (v) availability of carboxyl groups for further chemical modification; (vi) excellent colloidal stability and utility in cellular environments; (vii) low toxicity in cellular environments; and (viii) providing similar properties to other NP materials. Cumulative access to all these properties in a *single* ligand-coated QD has been extremely hard to achieve before. While some dendrimers do provide long-term stability and access to surfaces displaying multiple functional groups, this is again at the expense of significant size.[10,11] Maintaining a small hydrodynamic size is important for any potential *in vivo* utility. Equally important, imparting a zwitterionic nature to QD ligands has been repeatedly shown to prevent adsorption of serum proteins with concomitant increases in hydrodynamic diameter, a criteria that is deemed critical for renal clearance.[46,47,77−79]

Overall, we note a high degree of functional equivalence and zwitterionic character among **CL1**, **CL2**, and **CL4** suggesting that each is capable of imparting nearly the same properties to QDs. **CL3** served more as a control to verify that the simultaneous presence of both a carboxyl and tertiary amine are required

for optimal zwitterionic properties. However, its facile synthesis, small size, and relative *in vitro* robustness suggest that it is still useful for selected applications. The use of the high-affinity dithiol attachment domain should also allow these ligands to be applied to a number of other NP materials and surfaces including those derived from (or having shells of) Ag, Pd, and Pt.[7] In summary, the compact ligand series characterized here have a strong potential to expand QD and other NP capabilities in many biological applications.

■ ASSOCIATED CONTENT

Supporting Information. A schematic representation of cap exchange, a series of characterization data of the materials used, gel images of QD/His-tagged peptides conjugates, images for the cellular uptake study, DLS data of AuNPs, and detailed descriptions of the experimental conditions. This material is available free of charge via the Internet at http://pubs.acs.org.

■ AUTHOR INFORMATION

Corresponding Author
susumu@ccs.nrl.navy.mil; Igor.Medintz@nrl.navy.mil

■ ACKNOWLEDGMENT

The authors acknowledge NRL, the NRL NSI, DARPA, ONR, and ARO/DTRA for financial support. J.B.B.-C. acknowledges a Marie Curie IOF. W.J.H. gratefully acknowledges the NRC RAP postdoctoral fellowship program. W.R.A. is grateful to the Natural Sciences and Engineering Research Council of Canada (NSERC) for a postdoctoral fellowship. We thank Dr. M. Mauro at Life Technologies for providing a sample of custom Qdot 625 ITK organic QDs and S. MacDonald at ACD for assistance with pK_a determinations.

■ REFERENCES

(1) Gill, R.; Zayats, M.; Willner, I. *Angew. Chem., Int. Ed.* **2008**, *47*, 7602–7625.
(2) Boisselier, E.; Astruc, D. *Chem. Soc. Rev.* **2009**, *38*, 1759–1782.
(3) Yong, K.-T.; Roy, I.; Swihart, M. T.; Prasad, P. N. *J. Mater. Chem.* **2009**, *19*, 4655–4672.
(4) Algar, W. R.; Tavares, A. J.; Krull, U. J. *Anal. Chim. Acta* **2010**, *673*, 1–25.
(5) Biju, V.; Itoh, T.; Ishikawa, M. *Chem. Soc. Rev.* **2010**, *39*, 3031–3056.
(6) Zrazhevskiy, P.; Sena, M.; Gao, X. *Chem. Soc. Rev.* **2010**, *39*, 4326–4354.
(7) Thanh, N. T. K.; Green, L. A. W. *Nano Today* **2010**, *5*, 213–230.
(8) Jana, N. R. *Phys. Chem. Chem. Phys.* **2011**, *13*, 385–396.
(9) Medintz, I. L.; Uyeda, H. T.; Goldman, E. R.; Mattoussi, H. *Nat. Mater.* **2005**, *4*, 435–446.
(10) Oh, J. K. *J. Mater. Chem.* **2010**, *20*, 8433–8445.
(11) Smith, A. M.; Duan, H.; Rhyner, M. N.; Ruan, G.; Nie, S. *Phys. Chem. Chem. Phys.* **2006**, *8*, 3895–3903.
(12) Medintz, I. L.; Mattoussi, H. *Phys. Chem. Chem. Phys.* **2009**, *11*, 17–45.
(13) Algar, W. R.; Massey, M.; Krull, U. J. *Trends Anal. Chem.* **2009**, *28*, 292–306.
(14) Boeneman, K.; Prasuhn, D. E.; Blanco-Canosa, J. B.; Dawson, P. E.; Melinger, J. S.; Ancona, M.; Stewart, M. H.; Susumu, K.; Huston, A.; Medintz, I. L. *J. Am. Chem. Soc.* **2010**, *132*, 18177–18190.
(15) Rosenthal, S. J.; Chang, J. C.; Kovtun, O.; McBride, J. R.; Thomlinson, I. D. *Chem. Biol.* **2011**, *18*, 10–24.
(16) Mattoussi, H.; Mauro, J. M.; Goldman, E. R.; Anderson, G. P.; Sundar, V. C.; Mikulec, F. V.; Bawendi, M. G. *J. Am. Chem. Soc.* **2000**, *122*, 12142–12150.
(17) Medintz, I. L.; Berti, L.; Pons, T.; Grimes, A. F.; English, D. S.; Alessandrini, A.; Facci, P.; Mattoussi, H. *Nano Lett.* **2007**, *7*, 1741–1748.
(18) Sapsford, K. E.; Pons, T.; Medintz, I. L.; Higashiya, S.; Brunel, F. M.; Dawson, P. E.; Mattoussi, H. *J. Phys. Chem. C* **2007**, *111*, 11528–11538.
(19) Liu, W.; Howarth, M.; Greytak, A. B.; Zheng, Y.; Nocera, D. G.; Ting, A. Y.; Bawendi, M. G. *J. Am. Chem. Soc.* **2008**, *130*, 1274–1284.
(20) Lu, H.; Schöps, O.; Woggon, U.; Niemeyer, C. M. *J. Am. Chem. Soc.* **2008**, *130*, 4815–4827.
(21) Dennis, A. M.; Sotto, D. C.; Mei, B. C.; Medintz, I. L.; Mattoussi, H.; Bao, G. *Bioconjugate Chem.* **2010**, *21*, 1160–1170.
(22) Lee, J.; Kim, J.; Park, E.; Jo, S.; Song, R. *Phys. Chem. Chem. Phys.* **2008**, *10*, 1739–1742.
(23) Uyeda, H. T.; Medintz, I. L.; Jaiswal, J. K.; Simon, S. M.; Mattoussi, H. *J. Am. Chem. Soc.* **2005**, *127*, 3870–3878.
(24) Susumu, K.; Uyeda, H. T.; Medintz, I. L.; Pons, T.; Delehanty, J. B.; Mattoussi, H. *J. Am. Chem. Soc.* **2007**, *129*, 13987–13996.
(25) Mei, B. C.; Susumu, K.; Medintz, I. L.; Delehanty, J. B.; Mountziaris, T. J.; Mattoussi, H. *J. Mater. Chem.* **2008**, *18*, 4949–4958.
(26) Mei, B. C.; Susumu, K.; Medintz, I. L.; Mattoussi, H. *Nat. Protoc.* **2009**, *4*, 412–423.
(27) Susumu, K.; Mei, B. C.; Mattoussi, H. *Nat. Protoc.* **2009**, *4*, 424–436.
(28) Mei, B. C.; Oh, E.; Susumu, K.; Farrell, D.; Mountziaris, T. J.; Mattoussi, H. *Langmuir* **2009**, *25*, 10604–10611.
(29) Oh, E.; Susumu, K.; Goswami, R.; Mattoussi, H. *Langmuir* **2010**, *26*, 7604–7613.
(30) Oh, E.; Susumu, K.; Blanco-Canosa, J. B.; Medintz, I. L.; Dawson, P. E.; Mattoussi, H. *Small* **2010**, *6*, 1273–1278.
(31) Pons, T.; Uyeda, H. T.; Medintz, I. L.; Mattoussi, H. *J. Phys. Chem. B* **2006**, *110*, 20308–20316.
(32) Clapp, A. R.; Goldman, E. R.; Mattoussi, H. *Nat. Protoc.* **2006**, *1*, 1258–1266.
(33) Snee, P. T.; Chan, Y.; Nocera, D. G.; Bawendi, M. G. *Adv. Mater.* **2005**, *17*, 1131–1136.
(34) Li, J. J.; Wang, Y. A.; Guo, W.; Keay, J. C.; Mishima, T. D.; Johnson, M. B.; Peng, X. *J. Am. Chem. Soc.* **2003**, *125*, 12567–12575.
(35) Blackman, B.; Battaglia, D. M.; Mishima, T. D.; Johnson, M. B.; Peng, X. *Chem. Mater.* **2007**, *19*, 3815–3821.
(36) Blackman, B.; Battaglia, D. M.; Peng, X. *Chem. Mater.* **2008**, *20*, 4847–4853.
(37) Lehninger, A. L.; Nelson, D. L.; Cox, M. M. *Principles of Biochemistry*, 2nd ed.; Worth Publishers: New York, 1993.
(38) Berg, J.; Tymoczko, J.; Stryer, L. *Biochemistry*, 5th ed.; W. H. Freeman and Company: New York, 2002.
(39) Zhang, S.; Baker, J.; Pulay, P. *J. Phys. Chem. A* **2010**, *114*, 432–442.
(40) Hall, H. K., Jr. *J. Am. Chem. Soc.* **1957**, *79*, 5441–5444.
(41) Hermanson, G. T. *Bioconjugate Techniques*, 2nd ed.; Academic Press, Inc.: San Diego, CA, 2008.
(42) Duan, H.; Nie, S. *J. Am. Chem. Soc.* **2007**, *129*, 3333–3338.
(43) Tan, S. J.; Jana, N. R.; Gao, S.; Patra, P. K.; Ying, J. Y. *Chem. Mater.* **2010**, *22*, 2239–2247.
(44) Prasuhn, D. E.; Feltz, A.; Blanco-Canosa, J. B.; Susumu, K.; Stewart, M. H.; Mei, B. C.; Yakovlev, A. V.; Loukov, C.; Mallet, J. M.; Oheim, M.; Dawson, P. E.; Medintz, I. L. *ACS Nano* **2010**, *4*, 5487–5497.
(45) Rannard, S. P.; Davis, N. J. *Org. Lett.* **2000**, *2*, 2117–2120.
(46) Liu, W.; Choi, H. S.; Zimmer, J. P.; Tanaka, E.; Frangioni, J. V.; Bawendi, M. *J. Am. Chem. Soc.* **2007**, *129*, 14530–14531.
(47) Muro, E.; Pons, T.; Lequeux, N.; Fragola, A.; Sanson, N.; Lenkei, Z.; Dubertret, B. *J. Am. Chem. Soc.* **2010**, *132*, 4556–4557.
(48) Zhang, Y.; Schnoes, A. M.; Clapp, A. R. *ACS Appl. Mater. Interfaces* **2010**, *2*, 3384–3395.
(49) Stewart, M. H.; Susumu, K.; Mei, B. C.; Medintz, I. L.; Delehanty, J. B.; Blanco-Canosa, J. B.; Dawson, P. E.; Mattoussi, H. *J. Am. Chem. Soc.* **2010**, *132*, 9804–9813.

(50) *Tietz Textbook of Clinical Chemistry*, 3rd ed.; Burtis, C. A., Ashwood, E. R., Eds.; WB Saunders: Philadelphia, PA, 1998.
(51) Hochuli, E.; Döbeli, H.; Schacher, A. *J. Chromatogr.* **1987**, *411*, 177–184.
(52) Ueda, E. K. M.; Gout, P. W.; Morganti, L. *J. Chromatogr., A* **2003**, *988*, 1–23.
(53) Dif, A.; Boulmedais, F.; Pinot, M.; Roullier, V.; Baudy-Floc'h, M.; Coquelle, F. M.; Clarke, S.; Neveu, P.; Vignaux, F.; Le Borgne, R.; Dahan, M.; Gueroui, Z.; Marchi-Artzner, V. *J. Am. Chem. Soc.* **2009**, *131*, 14738–14746.
(54) Duan, H.; Kuang, M.; Wang, Y. A. *Chem. Mater.* **2010**, *22*, 4372–4378.
(55) Ghadiali, J. E.; Cohen, B. E.; Stevens, M. M. *ACS Nano* **2010**, *4*, 4915–4919.
(56) Prasuhn, D. E.; Blanco-Canosa, J. B.; Vora, G. J.; Delehanty, J. B.; Susumu, K.; Mei, B. C.; Dawson, P. E.; Medintz, I. L. *ACS Nano* **2010**, *4*, 267–278.
(57) Delehanty, J. B.; Bradburne, C. E.; Boeneman, K.; Susumu, K.; Farrell, D.; Mei, B. C.; Blanco-Canosa, J. B.; Dawson, G.; Dawson, P. E.; Mattoussi, H.; Medintz, I. L. *Integr. Biol.* **2010**, *2*, 265–277.
(58) Medintz, I. L.; Deschamps, J. R. *Curr. Opin. Biotechnol.* **2006**, *17*, 17–27.
(59) Susumu, K.; Medintz, I. L.; Delehanty, J. B.; Boeneman, K.; Mattoussi, H. *J. Phys. Chem. C* **2010**, *114*, 13526–13531.
(60) Medintz, I. L.; Clapp, A. R.; Mattoussi, H.; Goldman, E. R.; Fisher, B.; Mauro, J. M. *Nat. Mater.* **2003**, *2*, 630–638.
(61) Clapp, A. R.; Medintz, I. L.; Mauro, J. M.; Fisher, B. R.; Bawendi, M. G.; Mattoussi, H. *J. Am. Chem. Soc.* **2004**, *126*, 301–310.
(62) Pons, T.; Medintz, I. L.; Wang, X.; English, D. S.; Mattoussi, H. *J. Am. Chem. Soc.* **2006**, *128*, 15324–15331.
(63) Liu, Y.; Kim, M.; Wang, Y.; Wang, Y. A.; Peng, X. *Langmuir* **2006**, *22*, 6341–6345.
(64) Delehanty, J. B.; Mattoussi, H.; Medintz, I. L. *Anal. Bioanal. Chem.* **2009**, *393*, 1091–1105.
(65) Vivès, E.; Schmidt, J.; Pèlegrin, A. *BBA Rev. Cancer* **2008**, *1786*, 126–138.
(66) Fuchs, S. M.; Raines, R. T. *Biochemistry* **2004**, *43*, 2438–2444.
(67) Delehanty, J. B.; Medintz, I. L.; Pons, T.; Brunel, F. M.; Dawson, P. E.; Mattoussi, H. *Bioconjugate Chem.* **2006**, *17*, 920–927.
(68) Hoshino, A.; Hanada, S.; Manabe, N.; Nakayama, T.; Yamamoto, K. *IEEE Trans. Nanobiosci.* **2009**, *8*, 51–57.
(69) Rouhana, L. L.; Jaber, J. A.; Schlenoff, J. B. *Langmuir* **2007**, *23*, 12799–12801.
(70) Briñas, R. P.; Hu, M.; Qian, L.; Lymar, E. S.; Hainfeld, J. F. *J. Am. Chem. Soc.* **2008**, *130*, 975–982.
(71) Majzik, A.; Patakfalvi, R.; Hornok, V.; Dékány, I. *Gold Bull.* **2009**, *42*, 113–123.
(72) Cui, R.; Zhang, M.-X.; Tian, Z.-Q.; Zhang, Z.-L.; Pang, D.-W. *Nanoscale* **2010**, *2*, 2120–2125.
(73) Daniel, M. C.; Astruc, D. *Chem. Rev.* **2004**, *104*, 293–346.
(74) Breus, V. V.; Heyes, C. D.; Tron, K.; Nienhaus, G. U. *ACS Nano* **2009**, *3*, 2573–2580.
(75) Barglik-Chory, C.; Buchold, D.; Schmitt, M.; Kiefer, W.; Heske, C.; Kumpf, C.; Fuchs, O.; Weinhardt, L.; Stahl, A.; Umbach, E.; Lentze, M.; Geurts, J.; Muller, G. *Chem. Phys. Lett.* **2003**, *379*, 443–451.
(76) Zheng, Y.; Gao, S.; Ying, J. Y. *Adv. Mater.* **2007**, *19*, 376–380.
(77) Park, J.; Nam, J.; Won, N.; Jin, H.; Jung, S.; Jung, S.; Cho, S.-H.; Kim, S. *Adv. Funct. Mater.* **2011**, *21*, 1558–1566.
(78) Choi, H. S.; Liu, W.; Misra, P.; Tanaka, E.; Zimmer, J. P.; Ipe, B. I.; Bawendi, M. G.; Frangioni, J. V. *Nat. Biotechnol.* **2007**, *25*, 1165–1170.
(79) Choi, H. S.; Liu, W.; Liu, F.; Nasr, K.; Misra, P.; Bawendi, M. G.; Frangioni, J. V. *Nat. Nanotechnol.* **2010**, *5*, 42–47.